Palaeogeography, Palaeoclimatology, Palaeoecology 638 (2024) 112040

Contents lists available at ScienceDirect

Palaeogeography, Palaeoclimatology, Palaeoecology

journal homepage: www.elsevier.com/locate/palaeo

A benthic foraminifera perspective of the Late Miocene-Early Pliocene Biogenic Bloom at ODP Site 1085 (Southeast Atlantic Ocean)

Maria Elena Gastaldello [a,b,*], Claudia Agnini [a], Thomas Westerhold [c], Anna Joy Drury [d,e], Laia Alegret [b,f]

[a] Dipartimento di Geoscienze, Università degli Studi di Padova, Padova, Italy
[b] Departamento de Ciencias de la Tierra, Universidad de Zaragoza, Zaragoza, Spain
[c] MARUM - Center for Marine Environmental Sciences, University of Bremen, Bremen, Germany
[d] Department of Earth Sciences, University College London, London, UK
[e] School of Geography, Geology and the Environment, University of Leicester, Leicester, UK
[f] Instituto Universitario de Investigación en Ciencias Ambientales de Aragón, Universidad de Zaragoza, Zaragoza, Spain

ARTICLE INFO

Editor Name: Dr. Howard Falcon-Lang

Keywords:
Late Miocene
Early Pliocene
Biogenic Bloom
ODP Site 1085
Benthic foraminifera

ABSTRACT

The Late Miocene-Early Pliocene Biogenic Bloom (ca. 9.0–3.5 Ma) was a phase of high marine biological productivity documented globally at multiple ocean sites, related to an increase in nutrient input and/or a significant reorganization of nutrients in the oceans. Here, we studied the Biogenic Bloom at Ocean Drilling Program (ODP) Site 1085 in the Southeast Atlantic Ocean, additionally providing an updated age model based on calcareous nannofossil biostratigraphy. During the event, we identified four intervals characterised by distinct benthic foraminiferal assemblages, suggesting changes in paleoenvironmental/paleoceanographic conditions. The Biogenic Bloom extends from 8.1 to 3.0 Ma at Site 1085, as detected by different proxies such as linear sedimentation rates, carbonate mass accumulation rates, benthic foraminiferal indices and assemblage data. The inferred paleoenvironmental changes allowed us to differentiate four intervals within the Biogenic Bloom. From 8.1 to 5.2 Ma and from 3.8 to 3.0 Ma, the high benthic foraminiferal accumulation rates (BFARs) and the abundance of phytodetritus-exploiting taxa point to highly seasonal phytoplankton blooms. Between 5.2 and 4.8 Ma, we document short-term fluctuations between well-oxygenated conditions with transient input of phytodetritus and phases of low oxygen eutrophic conditions. Between 4.8 and 3.8 Ma, a decrease in opportunistic species and an increase in eutrophic taxa likely suggest a switch to a higher food supply to the seafloor. Our data shows that the onset of the Biogenic Bloom was synchronous with other global well-dated records and its end appears to align with other Atlantic records. Lastly, our findings support the hypothesis that the Biogenic Bloom was not a single productivity event, but a complex event made up of several short-lived, high-productivity regimes with different driving forces.

1. Introduction

The Late Miocene-Early Pliocene (11.6–3.6 Ma) interval is marked by a paleoceanographic phenomenon referred to as the "Late Miocene-Early Pliocene Biogenic Bloom" (from here on referred to as BB; Farrell et al., 1995). First described in the Equatorial Pacific Ocean (Farrell et al., 1995), the BB has been documented globally, especially in high-productivity areas and beneath upwelling regions in the Pacific Ocean (Berger et al., 1993; Grant and Dickens, 2002; Lyle et al., 2019) and in the Indian Ocean (Peterson et al., 1992; Dickens and Owen, 1999). At these sites, higher supply of biogenic $CaCO_3$ and other biogenic-related sediment components (e.g. opal, phosphorous) to the seafloor were documented around 9.0 and 3.5 Ma (Farrell et al., 1995; Dickens and Owen, 1999; Hermoyian and Owen, 2001; Grant and Dickens, 2002; Diester-Haass et al., 2005; Lyle et al., 2019). The anomalously high abundance of diatoms and species-specific dominance (e.g. Mikkelsen, 1990; Dickens and Barron, 1997) at several locations point to high productivity, and the dominance of suboxic and dysoxic benthic foraminifera (i.e. uvigerinids and buliminids) and changes in sediment geochemistry, such as a decreased Mn/Sc ratio, suggest low levels of dissolved oxygen in intermediate water depths (ca. 500–1500 m) (Dickens and Owen, 1994; Farrell et al., 1995; Nomura, 1995; Gupta and

* Corresponding author at: Dipartimento di Geoscienze, Università degli Studi di Padova, Padova, Italy.
E-mail address: mariaelena.gastaldello@phd.unipd.it (M.E. Gastaldello).

https://doi.org/10.1016/j.palaeo.2024.112040
Received 20 June 2023; Received in revised form 23 December 2023; Accepted 15 January 2024
Available online 18 January 2024

Thomas, 1999; Lyle et al., 2019). In the Atlantic, evidence for the BB was found in both high- and low-productivity areas, although the expression and timing off the BB was variable compared to the Pacific and Atlantic more ambiguous than in the Indian and Pacific Oceans (Diester-Haass et al., 2002, 2004; Drury et al., 2021). All these proxies point to a major increase in primary productivity, which seems to have lasted several millions of years. Two complementary hypotheses have been proposed to explain this phenomenon. The first one suggests that the BB was caused by an increase in the nutrient supply from the continents to the oceans, possibly related to enhanced weathering and the widespread continental aridification reported from vast areas during the Late Miocene (Berger et al., 1993; Berger and Stax, 1994; Delaney and Filippelli, 1994; Farrell et al., 1995; Filippelli, 1997; Hermoyian and Owen, 2001; Diester-Haass et al., 2006). The second one postulates that the BB resulted from a redistribution of nutrients within the oceans due to a reorganization of oceanic circulation (Farrell et al., 1995; Dickens and Owen, 1999; Diester-Haass et al., 2002).

The available data on the temporal and spatial extent of the BB leaves fundamental questions concerning its driving mechanisms, its consequences and the biotic response. Prior works have highlighted the regional heterogeneity in both the duration and manifestation of the BB (Dickens and Owen, 1999; Liao and Lyle, 2014; Lyle et al., 2019; Sutherland et al., 2019a; Drury et al., 2021; Gastaldello et al., 2023a). To achieve a more comprehensive understanding of this phenomenon, it is thus essential to discriminate the regional and global imprint of the BB. The Atlantic remains relatively unstudied in this respect.

Benthic foraminifera have been widely recognised as an essential proxy for reconstructing paleoenvironmental conditions in marine sediments due to their sensitivity to environmental changes and diverse ecological preferences (Gooday et al., 1992; Murray, 2000; Gooday, 2003; Murray, 2006; Jorissen et al., 2007). As a result, changes in their abundance, diversity, and assemblage composition can be used to reconstruct past environmental conditions, such as sea surface temperature, sea level, ocean circulation, and paleoproductivity (e.g. Jorissen et al., 2007). Quantitative analyses of benthic foraminiferal assemblages provide valuable insights into the local and regional processes that influenced the expression of the BB.

Ocean Drilling Program (ODP) Site 1085 was retrieved during ODP Leg 175 in the Southeast Atlantic Ocean and documents one of the most complete marine records spanning the Upper Miocene to the Lower Pliocene (Wefer et al., 1998). Previous studies on the BB focused on upwelling regions of the equatorial Indian and Pacific Oceans (Peterson et al., 1992; Berger et al., 1993; Farrell et al., 1995; Lyle et al., 2019), and limited information was available from coastal upwelling zones in the Atlantic Ocean (Diester-Haass et al., 2002, 2004). The thorough study of Site 1085 proposed here bridges these gaps by offering insights into changes in productivity during the Late Miocene to Early Pliocene in the Benguela Current upwelling. This site has been widely utilised in numerous studies related to oceanic circulation, climate variability, and biotic evolution (Christensen et al., 2002; Diester-Haass et al., 2002; Vidal et al., 2002; Diester-Haass et al., 2004; Robert et al., 2005; Westerhold et al., 2005; Dupont et al., 2013). Despite the wealth of data obtained from Site 1085, a detailed quantitative analysis of the benthic foraminiferal assemblages had yet to be conducted, something which our study focused specifically on rectifying. In this study, we analysed a continuous Late Miocene to Early Pliocene interval (10.9–3.0 Ma) at Site 1085 to test and refine the published age model (for Middle Miocene-Early Pliocene), to quantitatively and statistically analyse changes in benthic foraminiferal assemblage composition and paleoecology during the BB, and to provide a consistent paleoceanographic scenario. By combining our new assemblage data with sedimentary information, we fill a crucial gap in our understanding of the paleoceanography and productivity of the region during the Late Miocene to Early Pliocene.

2. Material and methods

2.1. Location and study material

Site 1085 (29°22.4665′S, 13°59.4064′E; 1713 m water depth, Fig. 1) was drilled in the Southeast Atlantic Ocean in the mid-Cape Basin during ODP Leg 175, and two holes were cored, Hole 1085A and Hole 1085B (Wefer et al., 1998). Site 1085 is located along the coast of South Africa, close to the river mouth of the perennial Orange River, which affects the area with variable runoff and discharge (Rogers and Bremner, 1991; Summerhayes et al., 1995). This site is influenced by plumes and filaments of cold, nutrient-rich waters flowing westward from the Benguela Upwelling Area (Berger et al., 2002) (Fig. 1).

The depth scale for Site 1085 is complex (see Westerhold et al., 2005). The depth scale follows the shipboard composite down to 1085B-29H-7, 84 cm (298.08 m composite depth - mcd). A composite is stitched together by multiple holes at a given site because in a single hole between consecutive cores there is always a recovery gap. At Site 1085, the succession deeper than 298.08 mcd was only recovered in a single-hole, preventing the constructions of a continuous composite record below this depth. To estimate the gaps in the record of Hole 1085A below the composite, XRF core scanning Fe data from Hole 1085A were correlated to the Hole 1085A Total Gamma Ray data (named SGR; abbreviation according to the original logging tool files) measured by the Natural Gamma Tool (NGT) string in the bore hole from 353.60 down to 555.04 m SGR log-depth (see Westerhold et al., 2005). From 555.82 down to 593.57 m log-depth, correlation to the SGR log was impossible, thus cores gaps were assumed to be in the order of 10% (see Westerhold et al., 2005). Finally, to connect the composite depth scale mcd with the SGR log-depth scale we offset the SGR log by 27.34 m down to match the mcd based on correlation to Core 1085B-29. The established depth scale is a mix of meters composite depth (mcd) and the SGR log depth, and is defined here as the revised mcd SGR or rmcdSGR. For clarity, we refer to the depth as m in the remainder of the text. For better reproducibility for future studies, mapping pairs for each core are given in Suppl. Table S1 to calculate the rmcdSGR depth below the shipboard mcd.

Sediments recovered from Site 1085 are described as two distinct lithostratigraphic units dominated by nannofossil ooze. Unit I (Hole A: 0–594.4 mbsf –meters below sea floor–, 0–656.06 rmcdSGR; Hole B: 0–321 mbsf, 0–354.11 rmcdSGR) has been subdivided into Subunit IA (Hole A: 0–98 mbsf, 0–108 rmcdSGR; Hole B: 0–83.9 mbsf, 0–93 rmcdSGR) and Subunit IB (Hole A: 89.2–594.4 mbsf, 99.2–656.06 rmcdSGR; Hole B: 83.9–321.2 mbsf, 93–354.31 rmcdSGR). The distinction between these two subunits reflect the decrease in foraminiferal content with increasing depth. Subunit IA extends from Core 175–1085A-1H through 10H at both holes, and Subunit IB extends from Cores 175-1085A-11H through 63× (Wefer et al., 1998). Unit II is a reddish brown, micro faulted and thinly laminated clay-rich nannofossil ooze. Unit II was identified from Core 175–1085A-64× downward (594.4–604 mbsf, 656.06–665.66 rmcdSGR; Wefer et al., 1998). Here, we studied a ca. 400 m-thick interval within subunit IB, from Core 15H to Core 55× (149 to 542.45 m), which spans from the Upper Miocene to the Lower Pliocene (approximately 10.9–3.0 Ma).

2.2. Oceanographic setting

Present-day surface circulation at Site 1085 is dominated by the Benguela Current (BC, Fig. 1). This northward current, combined with the SE trades, triggers the wide upwelling zone located between latitudes of about 16° and 34° S (Stramma and Peterson, 1989). High concentrations of nutrients and a prosperous biotic component, mostly fish and radiolarians, characterise the shelf edge (Summerhayes et al., 1995). Near the coast, diatom blooms are common due to the turbulent, nutrient-rich waters, while dinoflagellates and coccolithophores are more abundant over the middle and outer shelf (Pitcher et al., 1991). The onset of the Benguela upwelling circulation has been dated back to

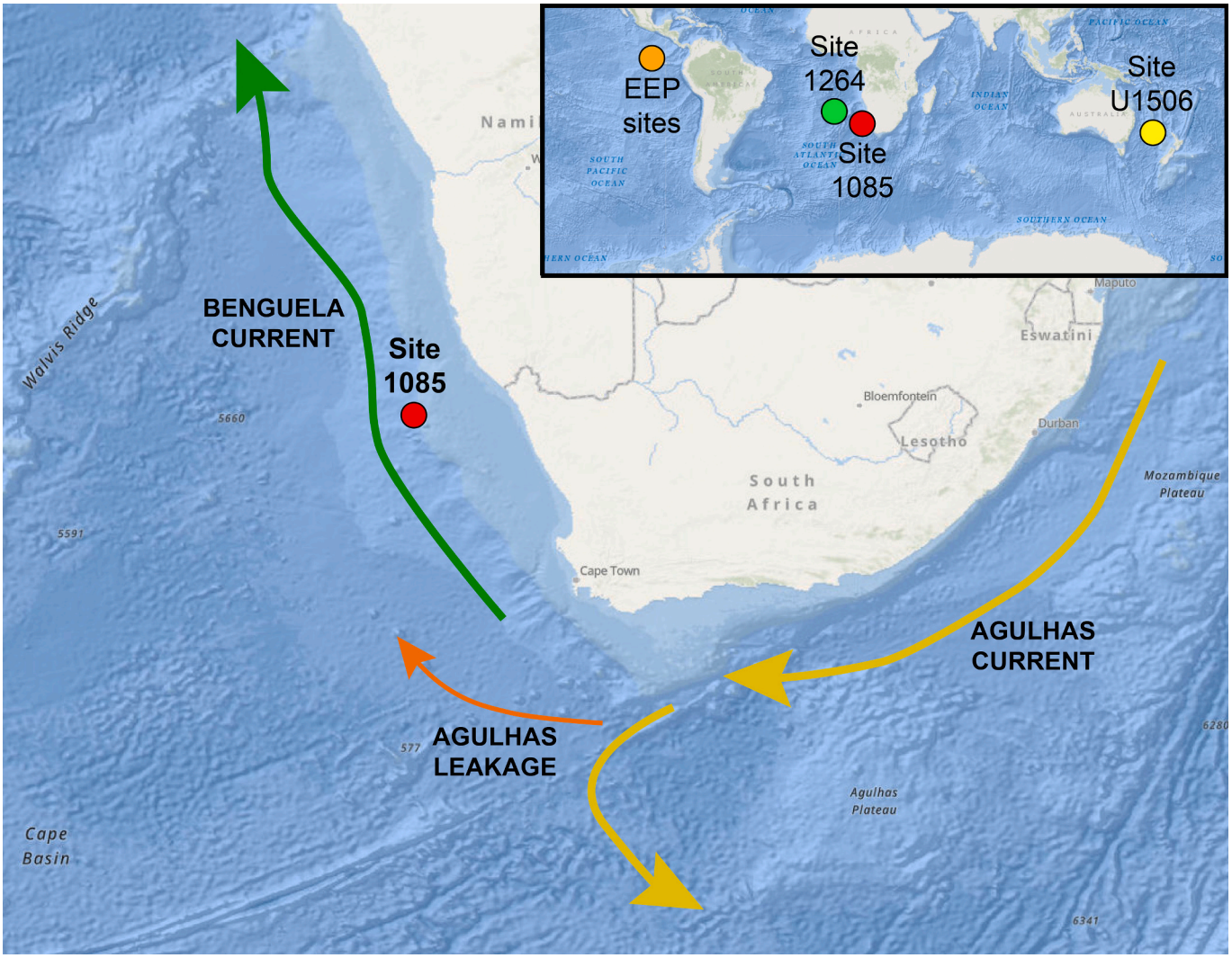

Fig. 1. Location map of ODP Site 1085 (red dot) and surface water circulation, including the Benguela current (green arrow), the Agulhas current (yellow arrow) and the Agulhas leakage (orange arrow) (https://maps.geomar.de/). In the upper-right corner map, location of IODP Site U1506 (yellow dot), ODP Site 1264 (green dot) (Drury et al., 2021), eastern equatorial Pacific stack (EEP sites, orange dot) (Lyle et al., 2019). (For interpretation of the references to colour in this figure legend, the reader is referred to the web version of this article.)

the Late Miocene (ca. 11.0–10.0 Ma), when cooling during Antarctic glacial periods strengthened, driving a northward shift in the BC and the subtropical anticyclone (Diester-Haass et al., 1990; Robert et al., 2005; Rommerskirchen et al., 2011). Benguelan upwelling is considered to have been responsible for the aridification of the Namibian desert (Linder, 2003; Bytebier et al., 2011; Dupont et al., 2011; Rommerskirchen et al., 2011). An oceanic component of the BC branches away from the coast and forms the eastern arm of the South Atlantic subtropical gyre, flowing into the South Equatorial Current (Shannon, 1985; Peterson and Stramma, 1991) (Fig. 1).

In this region, the hydrography between 500 and 2500 m water depth is characterised by the presence of the low salinity, nutrient-rich Antarctic Intermediate Water (AAIW) and the Upper Circumpolar Deep Water (UCDW), which is denoted by low oxygen and low carbonate ion concentrations (Diester-Haass et al., 2005; Rommerskirchen et al., 2011). In the Cape Basin below 2500 m and down to 4000 m water depth, the deep-water circulation is dominated by the highly saline, oxygen-rich, and nutrient-poor North Atlantic Deep Water (NADW; Wefer et al., 1996).

Potential changes in ocean circulation can have a significant impact on paleoenvironmental conditions. Benthic foraminifera distribution is not strictly tied to the physical and chemical parameters of the water masses (Jorissen et al., 2007). However, changes in ocean circulation can trigger changes in current velocity, salinity, bottom water oxygenation and carbonate saturation, which are some of the main environmental parameters that influence the distribution of benthic foraminifera species (Mackensen et al., 1995). Moreover, the wide upwelling zone in this area plays an important role, enhancing the flux of labile organic matter reaching the seafloor and influencing benthic foraminifera productivity (Guichard et al., 1999).

2.3. Calcareous nannofossils

A total of 91 samples were prepared between 542.45 and 149.00 m using the "smear slide" standard method (Bown and Young, 1998). The average sampling resolution is 4.2 m, which equals to ca. 80 kyr resolution (Suppl. Table S2; Gastaldello et al., 2023b). We performed calcareous nannofossil analyses to determine the abundance of selected taxa present in the fossil assemblages (Fig. 2), to this aim samples were examined under a Zeiss light microscope at 1250× magnification both at parallel and crossed nicols.

Calcareous nannofossil biostratigraphic (Fig. 3) results are based on semi-quantitative analyses, which consist of counting the number of specimens belonging to the same taxon present on an area of 1 mm^2

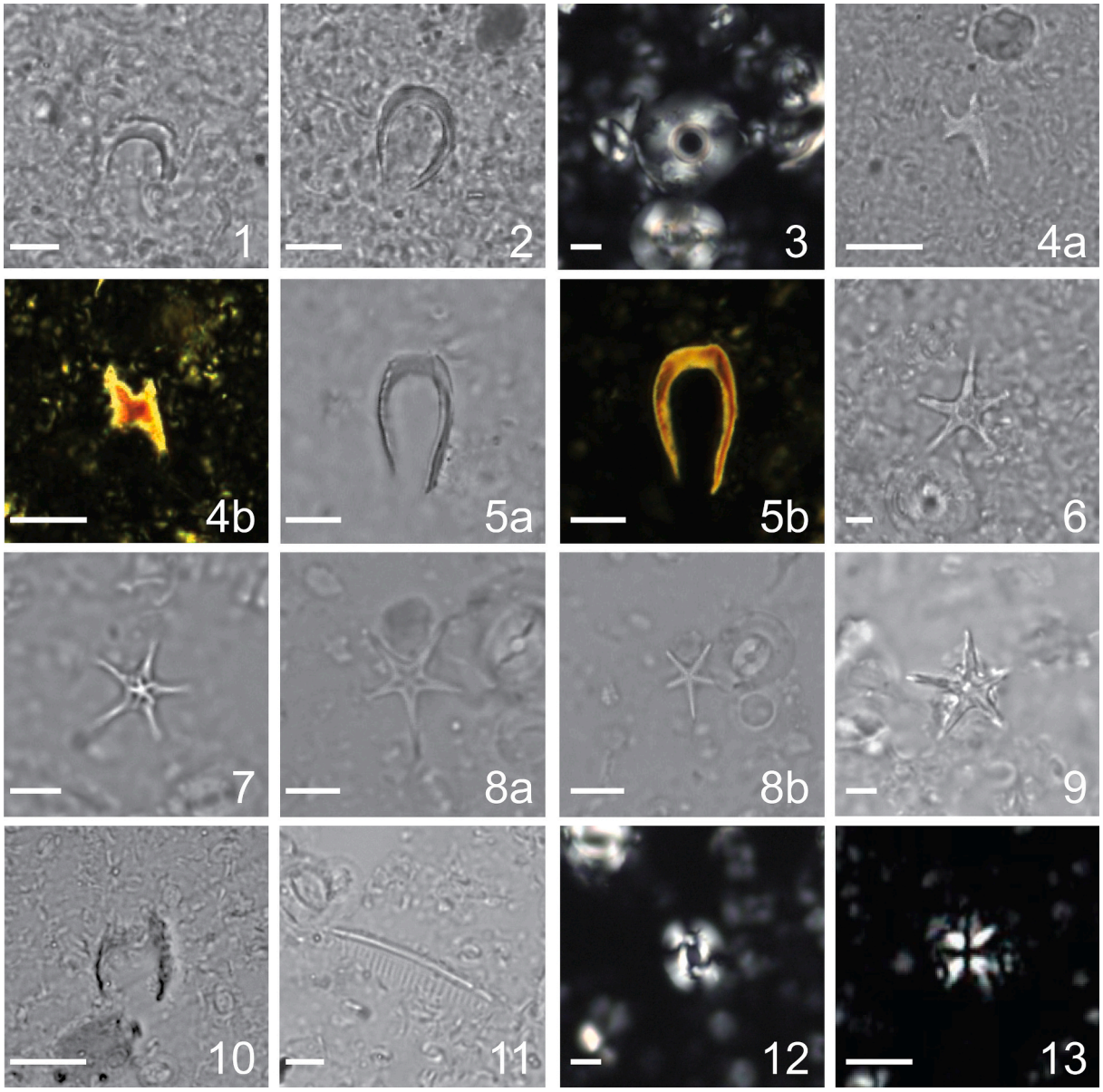

Fig. 2. Microphotographies of calcareous nannofossils from IODP Site U1506A. Optical polarizing microscope (1250 magnifications), parallel and crossed nicols. 1, *Amaurolithus primus* (sample 32H-6 W, 47–49 cm); 2, *Amaurolithus delicatus* (sample 16H-5 W, 36–38 cm); 3, *Calcidiscus macintyrei* (sample 46×-6 W, 50–52 cm); 4a-b *Ceratolithus atlanticus* (sample 22H-5 W, 87–89 cm); 5a-b, *Ceratolithus cristatus* (sample 22H-5 W, 87–89 cm); 6, *Discoaster asymmetricus* (sample 18H-1 W, 143–145 cm); 7, *Discoaster berggrenii* (sample 46×-6 W, 50–52 cm); 8a-b, *Discoaster hamatus* (sample 53×-2 W, 45–47 cm); 9, *Discoaster quinqueramus* (sample 34×-7 W, 34–36 cm); 10, *Nickilithus amplificus* (sample 40×-2 W, 50–52 cm); 11, *Orthorhabdus rugosus* (sample 46×-6 W, 50–52 cm); 12, *Reticulofenestra pseudoumbilicus* (sample 46×-6 W, 50–52 cm); 13, *Sphenolithus* spp. (sample 22H-5 W, 87–89 cm). All scale bars = 5 μm.

(Backman and Shackleton, 1983). We applied this method for biostratigraphic purposes, to provide the abundance pattern of marker species that are typically rare within the assemblages. The terms Base (B), Base common (Bc), Top (T), and Top common (Tc) are used to describe the biostratigraphic events (Agnini et al., 2014). To describe intervals in which a species or a genus disappear for a limited time, only to reappear further up the stratigraphic column, we adopted the terms Base absence (Ba) and Top absence (Ta) (Backman et al., 2012). The biostratigraphic schemes applied are those of Martini (1971), Okada and Bukry (1980), and Backman et al. (2012).

The determination of calcareous nannofossils is based on taxonomic concepts from different authors and sources (Farinacci and Howe, 1969-2022; Perch-Nielsen, 1985; Rio et al., 1990; Raffi and Flores, 1995; and the online atlas Nannotax). For the classification of *Amaurolithus*, *Nickilithus* and *Ceratolithus* we followed Raffi et al. (1998). For *Reticulofenestra pseudoumbilicus*, we counted the specimens with the length of the longer axis of the placolith >7 μm, as recommended by Rio et al. (1990) and Raffi and Flores (1995).

2.4. Benthic foraminifera quantitative analysis

A quantitative study on benthic foraminiferal assemblages was carried out in 33 samples between 542.45 and 149.00 m (Suppl. Table S3; Gastaldello et al., 2023b). Sampling resolution varied from 9 to 14 m, ca. 120 to 320 kyr, with the highest resolution across the BB (120 kyr). The dataset at Site 1085 has been acquired following the same methodology and applying the same taxonomic concepts used in Gastaldello et al. (2023a). Samples were dried in an oven at 40 °C, weighted to obtain bulk dry sample weight, disaggregated in water, washed through a 63 μm mesh sieve, and dried in an oven at 40 °C. For each sample,

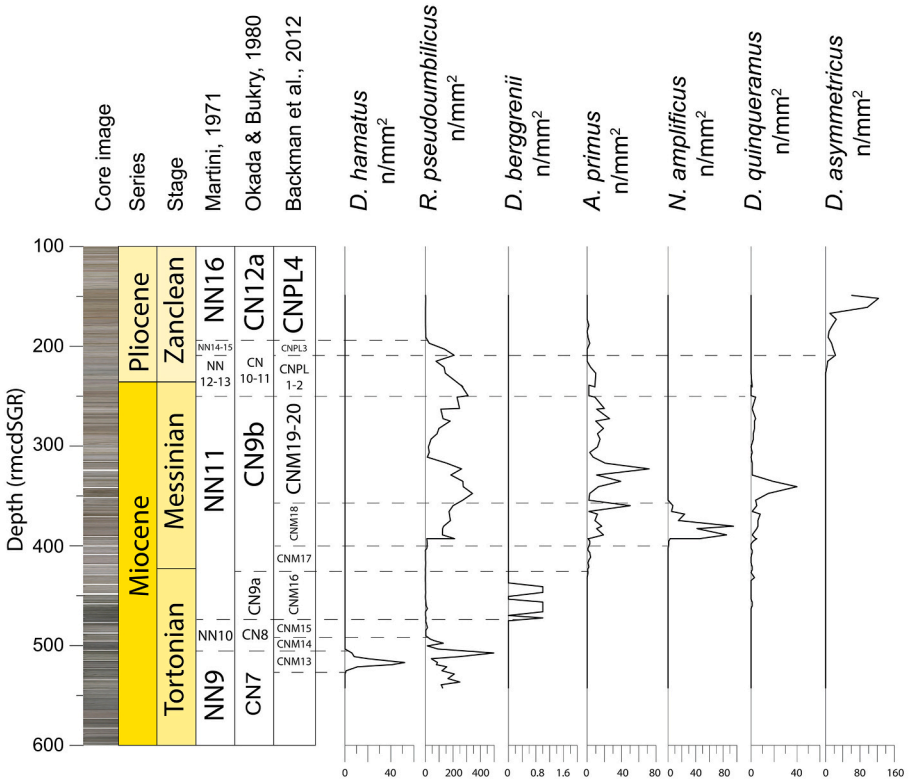

Fig. 3. Number of specimens of selected calcareous nannofossil taxa in a specific area (n/mm2) across the study interval at ODP Site 1085. On the left depth (m rmcdSGR) and Core image.

approximately 300 specimens of benthic foraminifera larger than 63 μm were picked and mounted on microslides for permanent record. The >63 μm fraction is considered to be more appropriate for a detailed analysis of the assemblages as several species produce small adult tests that would be lost using larger sieve sizes (125 μm, 150 μm, 250 μm). This fraction, by ensuring a lower number of lost specimens, allows for more reliable statistical analyses. Species identification follows Hayward and Buzas (1979), Van Morkhoven et al. (1986), Hermelin (1989), Kaminski and Gradstein (2005), Hayward et al. (2010), Hayward et al. (2013), and Holbourn et al. (2013). Photographs of the most representative specimens were obtained using the Scanning Electron Microscope imaging facilities at the University of Padova and the University of Zaragoza (Fig. 4 and Fig. 5). The specimens illustrated are deposited at the Natural Science Museum of the University of Zaragoza (Spain, repository numbers MPZ-2023/405 to MPZ-2023/426).

The relative abundance of each species (Fig. 6), the diversity (Fisher-α; Fisher et al., 1943) and the Shannon-Weaver H(S) indices (Murray, 1991), and the percentage of agglutinated and calcareous taxa were calculated (Fig. 7; Suppl. Table S4). We assigned each taxon to epifaunal or infaunal morphogroups following Corliss (1985), Jones and Charnock (1985), Corliss and Chen (1988), and Corliss (1991). By comparing fossil taxa with recent benthic foraminifera and analysing their morphotypes, probable microhabitat preferences can be inferred and paleoenvironmental parameters such as seafloor oxygenation, nutrient supply, or seasonal variations can be reconstructed (Bernhard, 1986; Jorissen et al., 1995; Fontanier et al., 2002). The infaunal-epifaunal ratio was used as a proxy for trophic conditions and oxygen levels in deep-sea environments. A high relative abundance of deep-sea infaunal species is considered to be indicative of eutrophic and/or low oxygen environments, while an increase in epifaunal taxa is likely indicative of oligotrophic conditions and/or high oxygen availability (Jorissen et al., 1995; Jorissen et al., 2007). To assess the assemblage changes across the BB, we grouped the relative abundance of species with similar paleoecological affinities, such as suboxic-dysoxic species (Bernhard, 1986; Kaiho, 1991) and phytodetritus exploiting taxa (PET; Gooday, 1988; Gooday, 1993; Suhr et al., 2003; Jorissen et al., 2007; Boscolo-Galazzo et al., 2015).

To further identify the environmental variables that may have controlled the distribution patterns of benthic foraminifera, we performed a hierarchical cluster analysis using the PAST software (Hammer et al., 2001) on a dataset of species with a relative abundance >5% in at least one sample, using the unweighted pair-group average algorithm (UPGMA) and the Pearson correlation (Suppl. Table S4). On the same dataset, Detrended Correspondence Analysis (DCA) in R-mode (species; Suppl. Fig. S1) and Q-mode (samples; Suppl. Fig. S2) were carried out to investigate the relationship between the changes in benthic foraminifera and the environmental variables (Hammer and Harper, 2005).

We calculated the benthic foraminiferal accumulation rates (BFAR; Suppl. Table S5) and coarse fraction accumulation rate (CFAR) using the equation proposed by Herguera and Berger (1991).

$$BFAR = (nr/g > 63\ \mu m * \%wt > 63/100) * LSR * DBD$$

$$CFAR = \%wt > 63\ \mu m * LSR * DBD$$

The BFAR is a semi-quantitative proxy for semi-quantitative estimation of paleoproductivity (Jorissen et al., 2007), and is expressed as counts $cm^{-2}\ kyr^{-1}$: nr/g > 63 μm is the number of benthic foraminifera per gram of sediment from the >63 μm fraction; %wt >63 μm is the weight percentage of foraminifera in >63 μm fraction of the sample; LSR is the linear sedimentation rate (cm/kyr), derived from the updated calcareous nannofossil biostratigraphy (see Sections 3.1 and 4.1); and DBD is the dry bulk density (g cm^{-3}) interpolated from the moisture and density (MAD) samples taken shipboard (Wefer et al., 1998). The CFAR was calculated by multiplying the amount (g) of coarse material (>63 μm fraction) per gram of sediment by the LSR and the DBD (Diester-Haass, 1995).

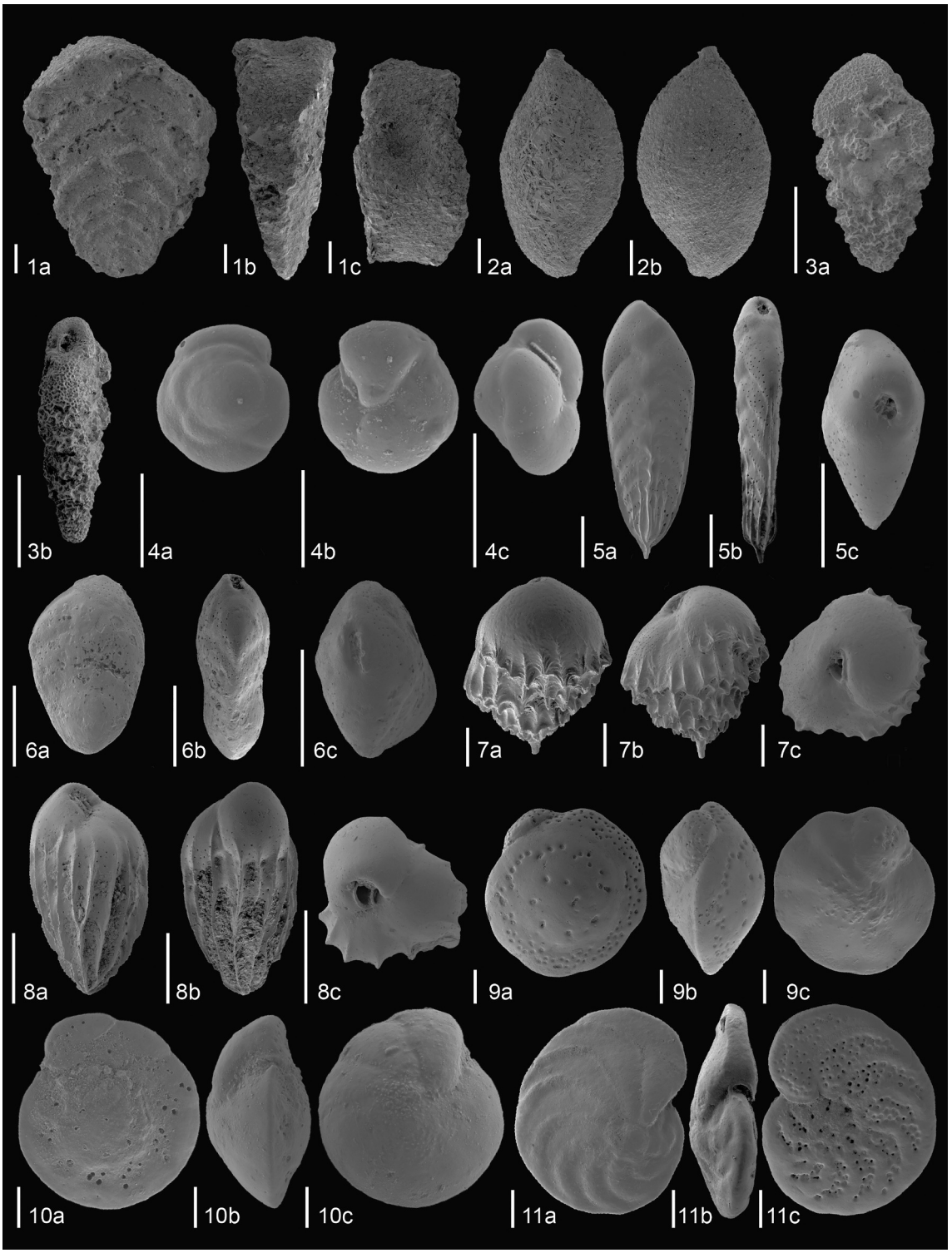

Fig. 4. SEM images of the most common benthic foraminiferal species at Site 1085. 1, *Textularia lythostrota* (sample 16H5, 36–38 cm), MPZ 2023/405: a) frontal side, b) lateral view; c) outline view; 2, *Sigmoilina schlumbergeri* (sample 24H2, 16–18 cm), MPZ 2023/406: a) frontal side; b) dorsal side; 3 *Abditodentrix pseudothalmanni* (sample 43 × 6, 46–48 cm), MPZ 2023/407: a) frontal side, b) lateral view; 4, *Alabaminella weddellensis* (sample 38 × 5, 61–63 cm), MPZ 2023/408: a) dorsal side, b), ventral side; c) apertural view; 5, *Bolivina subaenariensis* (sample 27H3, 110–112 cm), MPZ 2023/409: a) frontal side, b) lateral view; c) outline view; 6, *Bolivina spathulata* (sample 53 × 2, 47–49 cm), MPZ 2023/410: a) frontal side, b) lateral view; c) outline view; 7, *Bulimina striata* (sample 22H5, 87–89 cm), MPZ 2023/411: a) frontal side, b) dorsal side; c) outline view; 8, *Bulimina truncana* (sample 54 × 4, 30–32 cm), MPZ 2023/412: a) frontal side, b) dorsal side; c) outline view; 9, *Cibicidoides bradyi (*sample 50 × 4, 40–42 cm), MPZ 2023/413: a) dorsal side, b), side view; c) ventral side; 10, *Cibicidoides mundulus* (sample 54 × 4, 30–32 cm), MPZ 2023/414: a) dorsal side, b), side view; c) ventral side; 11, *Cibicidoides wuellestorfi* (sample 28H4, 12–14 cm), MPZ 2023/415: a) dorsal side, b), side view; c) ventral side. All scale bars = 100 μm.

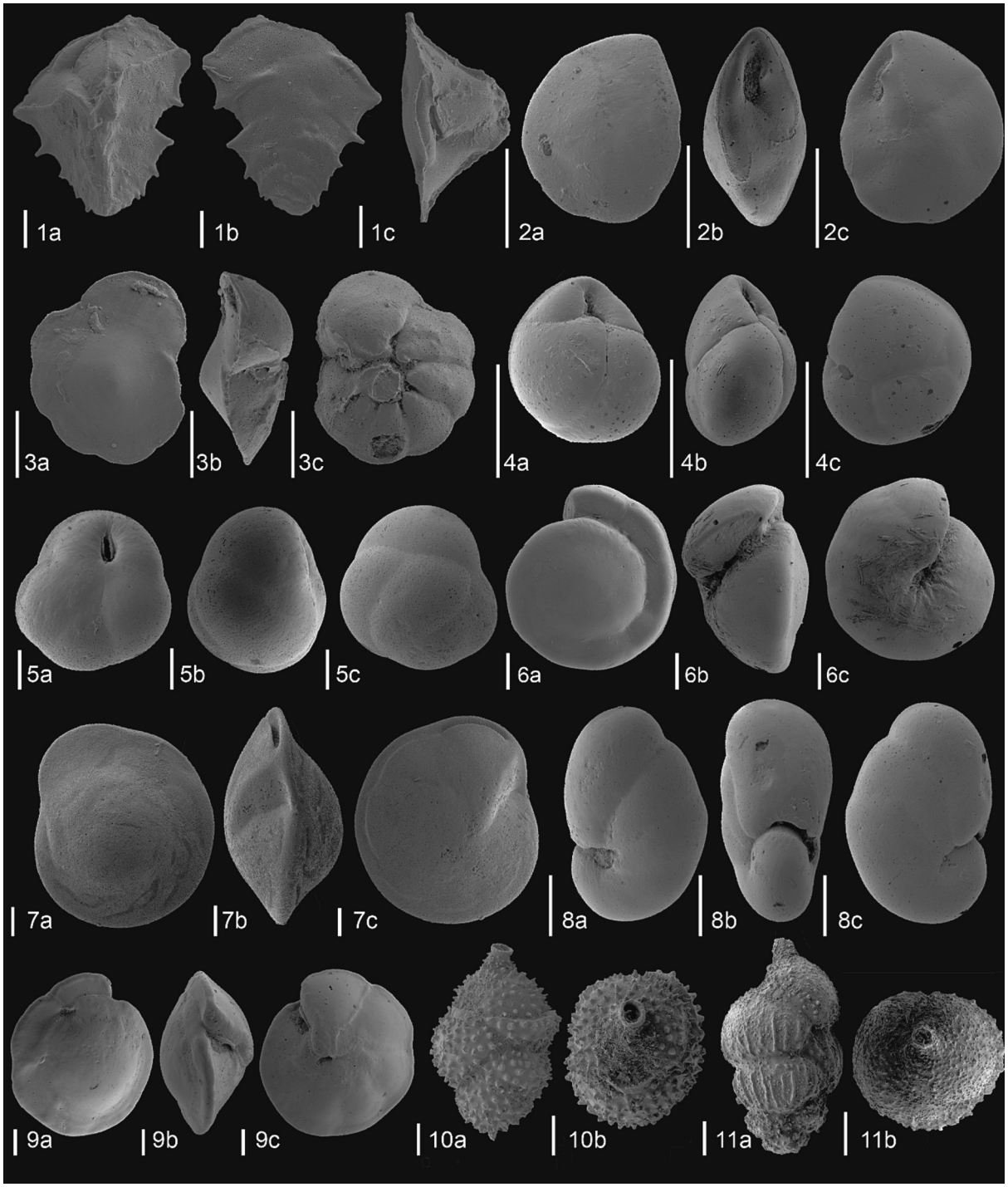

Fig. 5. SEM images of the most common benthic foraminiferal species at Site 1085. 1, *Ehrenbergina carinata* (sample 21H4, 131–133 cm), MPZ 2023/416: a) ventral side; b) dorsal side; c) apertural view; 2, *Epistominella exigua* (sample 16H5, 36–38 cm), MPZ 2023/417: a) dorsal side, b), side view; c) ventral side; 3, *Gavelinopsis lobatulus* (sample 16H5, 36–38 cm), MPZ 2023/418: a) dorsal side; b) side view; c) ventral side; 4, *Globocassidulina crassa* (sample 36 × 2, 44–46 cm), MPZ 2023/419: a) apertural view, b), side view; c) dorsal side; 5, *Globocassidulina subglobosa* (sample 34 × 7, 34–36 cm), MPZ 2023/420: a) apertural view, b), side view; c) dorsal side; 6, *Gyroidinoides orbicularis* (sample 20H4, 12–14 cm), MPZ 2023/421: a) dorsal side, b), side view; c) ventral side; 7, *Hoeglundina elegans* (sample 24H2, 16–18 cm), MPZ 2023/422: a) dorsal side; b) apertural view; c) ventral side; 8, *Nonionella* sp. (sample 22H5, 87–89 cm), MPZ 2023/423: a) ventral side, b), side view; c) dorsal side; 9, *Oridorsalis umbonatus* (sample 34 × 7, 34–36 cm), MPZ 2023/424: a) dorsal side, b), side view; c) ventral side; 10, *Uvigerina proboscidea* (sample 32H2, 14–16 cm), MPZ 2023/425: a) frontal view; b) outline view; 11, *Uvigerina peregrina* (sample 18H1, 144–145 cm), MPZ 2023/426: a) frontal view; b) outline view; All scale bars = 100 μm.

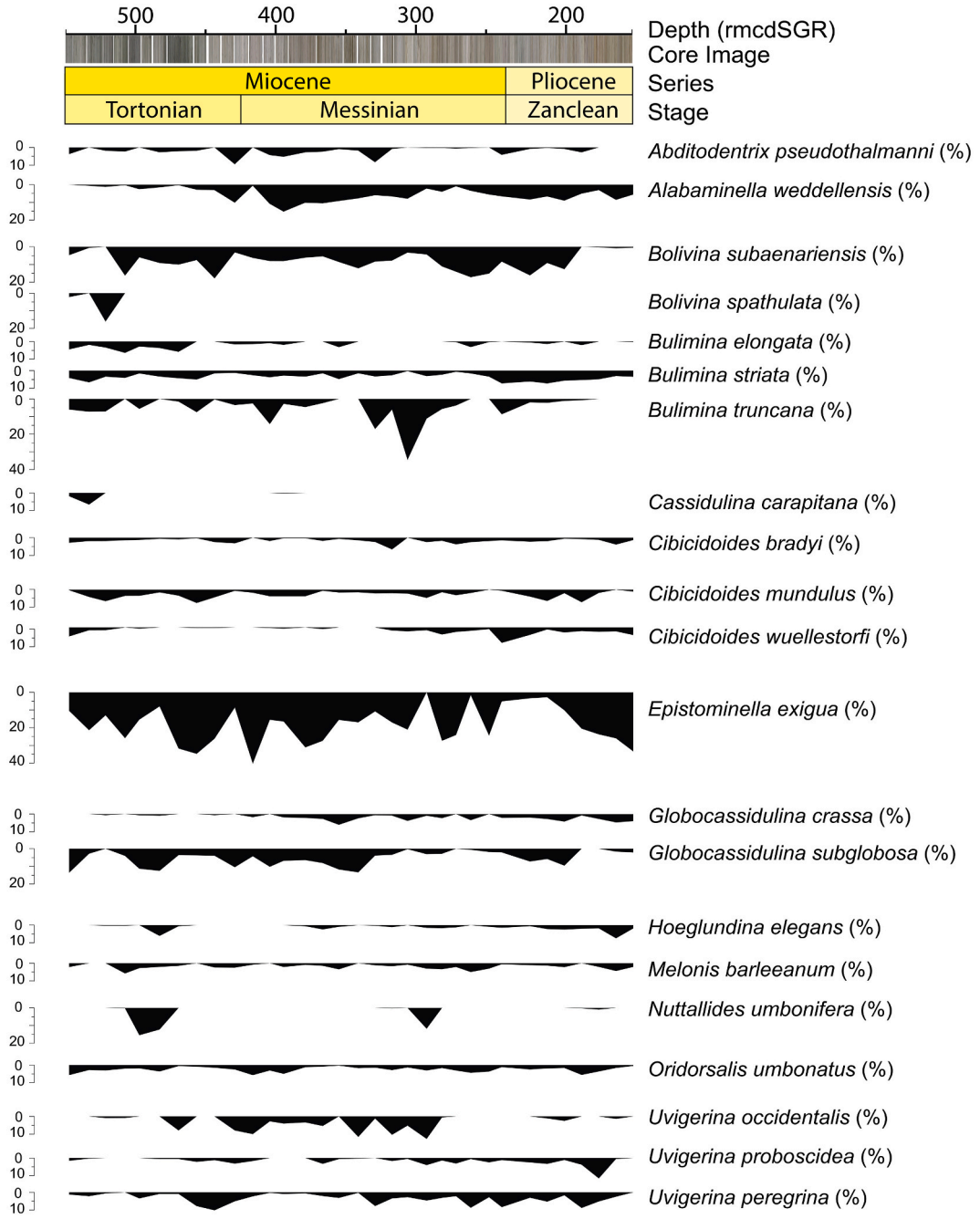

Fig. 6. Relative abundance of significant benthic foraminiferal species (>5% of the assemblages in at least one sample) at ODP Site 1085.

3. Results

3.1. Calcareous nannofossil biostratigraphy

Calcareous nannofossils are generally abundant and moderately to well preserved throughout the studied succession. For qualitative estimation of taxon abundance within the assemblage, we folllowed the methodology published in Sutherland et al. (2019b). Genus *Reticulofenestra* is abundant (>10–100 specimens per field of view) throughout the study interval while the abundance of *Amaurolithus*, *Discoaster* and *Nickilithus* ranges from few (1 specimen per 1–10 fields of view) to common (>1–10 specimens per field of view). *Calcidiscus* and *Ceratolithus* are also present. Semiquantitative counts (n/mm^{-2}) have not been performed for *Calcidiscus macintyrei* and *Sphenolithus abies*, for which we only provide presence-absence data in all the study samples. The selected biohorizons are listed from youngest to oldest and summarised in Table 1. For each biohorizon, the following information is provided regarding its usage in the adopted biostratigraphic schemes, the position of the event at Site 1085, the characteristics of the event in terms of abundance pattern, and a reliability assessment of the event compared to literature data.

3.1.1. Top Sphenolithus spp.

The disappearance (Top) of the genus *Sphenolithus* is not used to define a zonal boundary, but it provides a useful secondary biostratigraphic datum (Backman et al., 2012). This event is usually found to lie within Zone CNPL4 (Backman et al., 2012), shortly after the final disappearance (Top) of *R. pseudoumbilicus,* with an estimated age of 3.61 Ma (Raffi et al., 2020). At Site 1085, this biohorizon has been recognised between samples 1085A-19H-3W, 127–129 cm and 1085A-

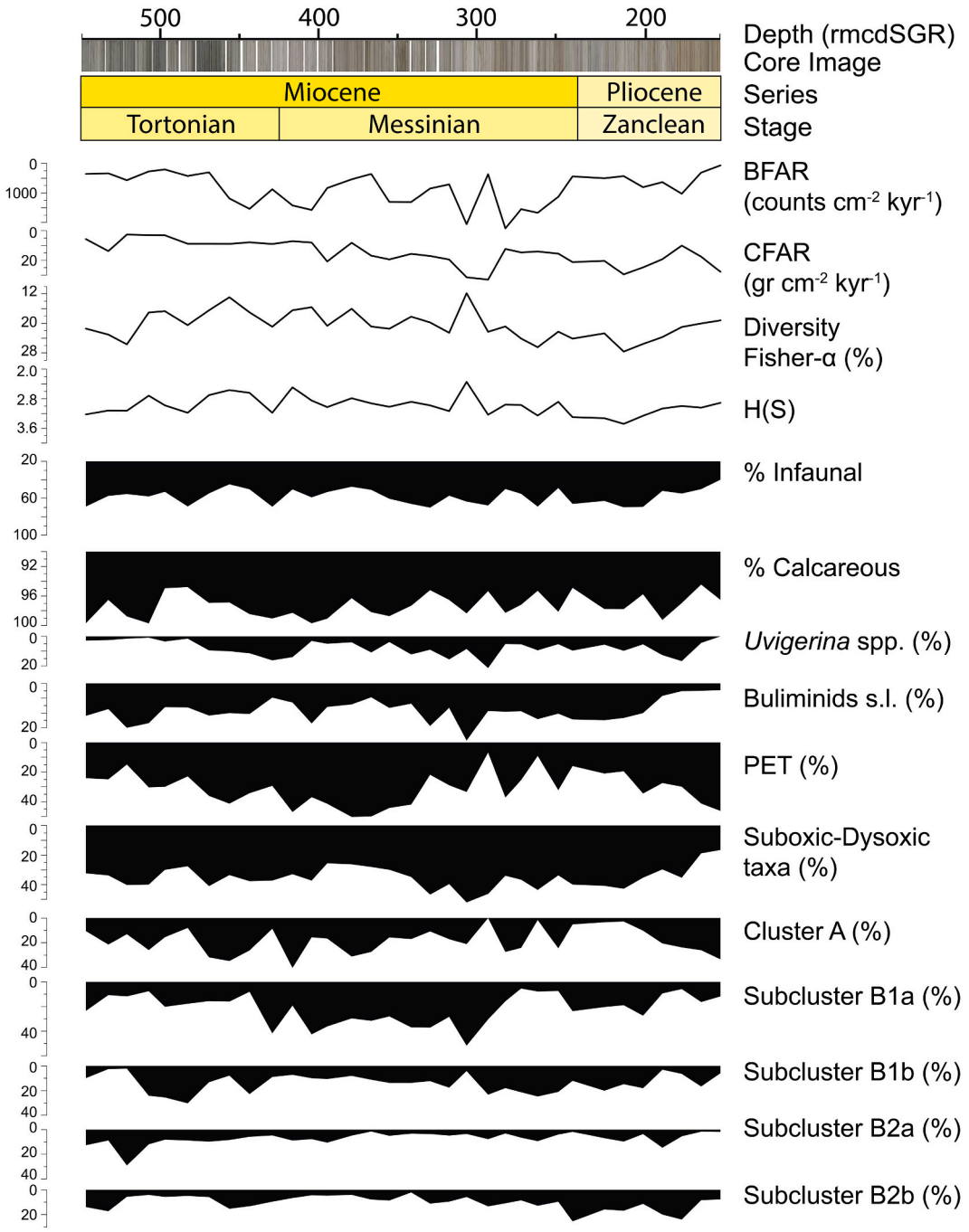

Fig. 7. Quantitative analysis of benthic foraminiferal assemblages at ODP Site 1085, plotted against depth (rmcdSGR): benthic foraminifera accumulation rates (BFAR), coarse fraction accumulation rates (CFAR), Fisher-α diversity index, Shannon-Weaver H(S) heterogeneity index, infaunal morphogrups, percentage of calcareous taxa, relative abundance of *Uvigerina* spp., buliminids *s.l.,* phytodetritus exploiting taxa (PET), dysoxic-suboxic taxa and relative abundance of clusters A and subclusters.

18H-5W, 143–145 cm, at 182 (±3.00) m.

3.1.2. Top Reticulofenestra pseudoumbilicus

The disappearance (Top) of *R. pseudoumbilicus,* observed at 194.00 (±3.00) m at Site 1085, marks the base of Subzone CN12a (Okada and Bukry, 1980), of Zone NN16 (Martini, 1971) and of Zone CNPL4 (Backman et al., 2012). At Site 1085, this event occurs between samples 1085B-20H-4W, 53–55 cm and 1085A-20H-2W, 11–13 cm, at 194 (± 3.00) m, where the abundance of *R. pseudoumbilicus* drops from 150 to 200 forms to ca. 1 specimen per mm^2.

The Top of *R. pseudoumbilicus* is considered to be a reliable biohorizon with an estimated age of 3.82 Ma (Backman et al., 2012), and it has been reported to be synchronous in several studies (e.g., Backman and Shackleton, 1983; Young, 1990; Shackleton et al., 1995). Raffi et al. (2020) evaluated this biohorizon with the maximum degree of reliability, defining it as "isochronous worldwide".

3.1.3. Base common Discoaster asymmetricus

The Base common of *D. asymmetricus* occurs between samples 1085 A-22H-4 W, 9–11 cm and 1085B-21H-4 W, 131–133 cm, at 212.00 (± 3.00) m. This event marks the base of Zone NN14 and Zone NN15 (Martini, 1971), the base of Subzone CN11b (Okada and Bukry, 1980),

Table 1
Biohorizons used for biostratigraphy at ODP Site 1085. From left to right: type of event (T, top; Ta, Top absence; B, base; Ba, Base absence; Bc, Base common), species and the relative biozones they define (Martini, 1971; Okada and Bukry, 1980; Backman et al., 2012), samples and their depths, and the age associated to each biohorizon (GTS2020; Raffi et al., 2020).

Event	Species	Biozone Okada and Bukry, 1980	Biozone Martini, 1971	Biozone Backman et al., 2012	Depth top (rmcdSGR)	Depth bottom (rmcdSGR)	Depth midpoint (rmcdSGR)	Depth error (m)	Sample top	Sample base	Age (Ma) GTS2020
T	*Sphenolithus* spp.				179.00	185.00	182.00	3.00	1085A-18H-5 W, 143–145 cm	1085A-19H-3 W, 127–129 cm	3.61
T	*Reticulofenestra pseudoumbilicus*	CN12a	NN16	CNPL4	191.00	197.00	194.00	3.00	1085A-20H-2 W, 11–13 cm	1085B-20H-4 W, 53–55 cm	3.82
Bc	*Discoaster asymmetricus*	CN11b	NN15 NN14	CNPL3	221.00	227.00	224.00	3.00	1085B-21H-4 W, 131–133 cm	1085A-22H-4 W, 9–11 cm	4.04
T	*Amaurolithus primus*				215.00	221.00	218.00	3.00	1085A-22H-4 W, 9–11 cm	1085B-22H-5 W, 87–89 cm	4.50
T	*Discoaster quinqueramus*	CN10a	NN12	CNM20	249.56	251.00	250.28	0.72	1085A-25H-2 W, 96–98 cm	1085A-25H-3 W, 84–86 cm	5.53
T	*Nickilithus amplificus*			CNM19	354.32	359.79	357.06	2.74	1085A-36×-2 W, 44–46 cm	1085A-36×-6 W, 44–46 cm	5.98
B	*Nickilithus amplificus*			CNM18	398.13	402.45	400.29	2.16	1085A-40×-6 W, 50–52 cm	1085A-41×-2 W, 50–52 cm	6.82
Ta	*Reticulofenestra pseudoumbilicus*				402.45	404.53	403.49	1.04	1085A-41×-2 W, 50–52 cm	1085A-41×-4 W, 50–52 cm	7.10
B	*Amaurolithus primus*	CN9b		CNM17	426.87	431.87	429.37	2.50	1085A-43×-6 W, 50–52 cm	1085A-44×-2 W, 48–50 cm	7.45
B	*Discoaster quinqueramus*		NN11		460.24	462.99	461.62	1.37	1085A-47×-2 W, 50–52 cm	1085A-47×-2 W, 50–52 cm	8.10
B	*Discoaster berggrenii*	CN9a		CNM16	466.12	469.82	467.97	1.85	1085A-47×-6 W, 35–37 cm	1085A-48×-4 W, 48–50 cm	8.29
Ba	*Reticulofenestra pseudoumbilicus*			CNM15	490.29	493.47	491.88	1.59	1085 A-50×-2 W, 48–50 cm	1085 A-50×-4 W, 40–42 cm	8.80
T	*Discoaster hamatus*	CN8a	NN10	CNM14	503.44	507.43	505.44	1.99	1085A-51×-6 W, 45–47 cm	1085A-52×-2 W, 46–48 cm	9.61
B	*Discoaster hamatus*	CN7	NN9	CNM13	525.23	528.52	526.87	1.65	1085A-54×-2 W, 50–52 cm	1085A-54×-4 W, 30–32 cm	10.57

and the base of Zone CNPL3 (Backman et al., 2012). At Site 1085, with the beginning of this biozone, the representative species of the genus *Amaurolithus* (i.e., *Amaurolithus primus* and *Amaurolithus delicatus*) decrease neatly, and their abundance drops to 1–2 specimens per mm^2.

3.1.4. Top *Amaurolithus primus*

The disappearance (Top) of *A. primus* is not used in any of the biozonations adopted in this work but it has been reported to occur within Zone CNPL2 (Backman et al., 2012). This event occurs between samples 1085B-22H-5W, 87–89 cm and 1085A-22H-4W, 9–11 cm, at 218.00 (±3.00) m. The position of this biostratigraphic event between the Top of *D. quinqueramus* and the Base Common of *D. asymmetricus* confirms the literature ranking (Backman et al., 2012).

At Site 1085 the Top of *A. primus* shows a discontinuous presence between 221 and 179 m. The disappearance interval of *A. primus* is reported to be characterised by generally low and uneven occurrences (Backman et al., 2012), making it inappropriate to define a zonal boundary. Moreover, Raffi and Flores (1995) reported that in different studies (i.e. Berggren et al., 1985) the extinction pattern of some ceratolithids species (including *A. primus*) has been inadequately documented, leading to a discrepancy in the age estimate for the disappearance of these species. Raffi et al. (2020) evaluated this biohorizon with the lowest degree of reliability, defining it as poorly defined and proven to be diachronous. For these reasons, we decided not to use it as a tie-point in the age model.

3.1.5. Base and Top of *Ceratolithus acutus*

The total range of *C. acutus* defines Subzone CN10b (Okada and Bukry, 1980) and Zone CNPL1 (Backman et al., 2012). Moreover, the Top of *C. acutus* marks the base of Zone NN13 (Martini, 1971). Since no specimens of this taxon were encountered at Site 1085, we combined Zone NN12 with Zone NN13 (Martini, 1971), and Zone CNPL1 with Zone CNPL2 (Backman et al., 2012). The scarce occurrence of *Ceratolithus* spp. is documented also in the shipboard data (Wefer et al., 1998).

3.1.6. Top *Discoaster quinqueramus*

The disappearance (Top) of *D. quinqueramus* marks the base of Zone NN12 (Martini, 1971), Subzone CNM10a (Okada and Bukry, 1980) and

Zone CNM20 (Backman et al., 2012). The final range of *D. quinqueramus* displays a tail of scattered abundances, and the precise position of the final exit of this taxon has been tentatively placed at 250.28 (± 0.72) m, between samples 1085A-25H-3W, 84–86 cm and 1085A-25H-2W, 96–98 cm. In the literature, the Top of *D. quinqueramus* is considered as a reliable biohorizon with an estimated age of 5.53 Ma (Backman et al., 2012). In this study, however, specimens ascribable to *Discoater* species are extremely rare, and the positioning of this event is highly uncertain which is the main reason why we decided not to use this biohorizon in our age model.

3.1.7. Base and Top of Nickilithus amplificus

The total range of *N. amplificus* defines Zone CNM18 of Backman et al. (2012). *Nickilithus amplificus* appears between samples 1085A-41×-2W, 50–52 cm and 1085A-40×-6W, 50–52 cm, at 400.29 (±2.16) m and disappears between samples 1085A-36×-6W, 44–46 cm and 1085A-36×-2W, 44–46 cm, at 357.06 (±2.74) m. This taxon range zone coincides with the upper part of Zone 11 (Martini, 1971) and with the middle part of Subzone CN9b (Okada and Bukry, 1980). The disappearance of *N. amplificus* defines the base of Zone CNM19 of Backman et al. (2012).

Nickilithus amplificus presents the typical short stratigraphic range consistent with the literature (Raffi et al., 1998), and a continuous abundance pattern. Our datum is consistent with the shipboard result (Wefer et al., 1998), where the Base of *N. amplificus* was placed at 395.27 m and the Top at 356.96 m. Focusing on the appearance pattern of the *Amaurolithus – Nicklithus – Ceratolithus* lineage (Raffi et al., 1998), the first appearance (Base) of *N. amplificus* documented after the appearance of genus *Amaurolithus* (i.e. *A. primus* and *A. delicatus*), and the Top of *N. amplificus* positioned before the first appearance of the genus *Ceratolithus* (i.e. *Ceratolithus atlanticus* and *Ceratolithus cristatus*), confirm the reliability of this event. Moreover, Raffi and Flores (1995) and Backman and Raffi (1997) showed that the base of this taxon is a reliable biostratigraphic event and that it appears to be isochronous among the equatorial Indian, Pacific and Atlantic Oceans.

3.1.8. Top absence Reticulofenestra pseudoumbilicus

The Top absence of *R. pseudoumbilicus* marks the end of the paracme interval of this taxon at 403.49 (± 1.04) m. This biohorizon is not used by any of the biozonations applied in this study but is reported to occur within Zone CNM17, with an estimated age of 7.09 Ma (Backman et al., 2012). At Site 1085, *R. pseudoumbilicus* shows a low (<10–15 specimens per mm^2) and sometimes discontinuous abundance pattern between 491.88 (± 1.59) and 403.49 (± 1.04) m. The end of the paracme event is located between sample 1085 A-41×-4 W, 50–52 cm and sample 1085A-41×-2 W, 50–52 cm, where the abundance of *R. pseudoumbilicus* starts to increase and reaches values around 150–250 specimens per mm^2, values that are comparable to the abundance prior to the paracme interval (Fig. 3).

For biostratigraphic purposes and according to some authors (Rio et al., 1990; Raffi and Flores, 1995) the description of *R. pseudoumbilicus* is based on a strictly morphometric parameter that includes only specimens with a long axis > 7 μm. However, it is becoming increasingly clear that light intensity, Mg/Ca ratio, nutrient availability, temperature and other factors could have played a role in terms of change in coccolith morphology (Faucher et al., 2020). This would in turn imply a possible diachronism due to different environmental conditions at different locations. In addition, Raffi et al. (2020) classified this event as "rather indistinct" and not well-defined.

3.1.9. Base of Amaurolithus primus

The Base of *A. primus*, which coincides with the base of the genus, marks the base of Subzone CN9b of Okada and Bukry (1980) and the base of Zone CNM17 of Backman et al. (2012). At Site 1085, this event is positioned between sample 1085 A-44×-2 W, 48–50 cm and sample 1085 A-43×-6 W, 50–52 cm at 429.37 (± 2.50) m. At the base of the range, between 429.37 and 390.92 m, we observed a low abundance of *A. primus*, with an average of 2 specimens per mm^2, followed by an upward increase, reaching an average of 15 specimens per mm^2. The highest occurrence is located in the middle part of the studied interval, with a peak of 72 specimens per mm^2 at 322.90 m. The position of the base of *A. primus* at Site 1085 between the base of *D. berggrenii* (467.97 m) and the appearance of *A. delicatus* (415.67 m), as typically reported in the literature (Raffi et al., 1998; Backman et al., 2012), confirms the ranking of this event.

3.1.10. Base of Discoaster quinqueramus

It marks the base of Zone NN11 of Martini (1971). At Site 1085, this event occurs slightly after the appearance of *D. berggrenii*, which marks the base of Zone CN9a (Okada and Bukry, 1980) and CNM16 (Backman et al., 2012). The Base of this taxon was recognised between samples 1085A-47×-2W, 50–52 cm and 1085A-47×-2W, 50–52 cm (461.62 ± 1.37 m). When it enters the record and up to 396.73 m, *Discoaster quinqueramus* shows a rare and uneven distribution pattern with an average abundance of 1 specimen per mm^2. Its abundance remains low with an average of 5 specimens per mm^2 until 350.93 m, where *D. quinqueramus* shows an increase in abundance, reaching a maximum of 40 specimens per mm^2 at 340.75 m. Raffi et al. (2020) define this event as poorly reliable.

3.1.11. Base of Discoaster berggrenii

The appearance of *D. berggrenii* at 467.97 (± 1.85) m marks the base of Subzone CNM9a of Okada and Bukry (1980), and the base of Zone CNM16 of Backman et al. (2012). At Site 1085, *D. berggrenii* is rare and occurs only in the lower part of the study interval, with an average abundance of 1 specimen per mm^2. Raffi et al. (1998) proposed that both *D. quinqueramus* and *D. berggrenii* originated from *Discoaster bellus*, its simple structure evolved towards more ornamented taxa such as *D. berggrenii* and *D. quinqueramus*. The evolution along of this lineage is gradual and thus characterised by the presence of intermediate forms, which makes it difficult to precisely identify the first appearance of *D. berggrenii* and the degree of synchrony/diachrony of this event in different areas (see discussion in Backman and Raffi, 1997 for details). In this study *D. berggrenii* appears slightly before *D. quinqueramus*, between samples 1085A-48×-4W, 48–50 cm and 1085A-47×-6W, 35–37 cm (Fig. 3). The low abundance and scattered occurrence of *D. berggrenii* at Site 1085 makes this event an unreliable biohorizon, in agreement with the literature (Raffi et al., 2006; Zeeden et al., 2013).

3.1.12. Base absence of Reticulofenestra pseudoumbilicus

The Base absence of *R. pseudoumbilicus* at 491.88 (± 1.59) m marks the base of Zone CNM15 (Backman et al., 2012). At Site 1085, the beginning of the paracme event is located between sample 1085A-50×-4W, 40–42 cm and sample 1085A-50×-2W, 48–50 cm, where the abundance of this species drops from ca. 100–200 to 10–15 specimens per mm^2. This interval of absence is also referred to as the "*R. pseudoumbilicus* paracme", and it has been documented in the Indian, Pacific and Atlantic Oceans (Rio et al., 1990; Young, 1990; Gartner, 1992; Takayama, 1993; Raffi and Flores, 1995; Backman and Raffi, 1997). The position of Base absence of the *R. pseudoumbilicus* falls between the Top of *D. hamatus* (526.98 m) and the Base of *D. berggrenii* (467.97 m), as documented in previous publications (Raffi et al., 2006; Backman et al., 2012), indicating a coherent ranking for this event also at Site 1085.

3.1.13. Base and top of Discoaster hamatus

The Base of *D. hamatus* at 526.98 (± 1.54) m marks the base of Zone CN7 (Okada and Bukry, 1980), of Zone NN9 (Martini, 1971), and the base of Zone CNM13 (Backman et al., 2012). This species has a short stratigraphic range that was observed in the lower part of the study interval. The first occurrence (Base) is located between samples 1085A-54×-4W, 30–32 cm and 1085A-54×-2W, 50–52 cm. The extinction

(Top) of *D. hamatus* has been detected between sample 1085A-52×-2W, 46–48 cm and sample 1085A-51×-6W, 45–47 cm (505.44 ± 1.99), and denotes the base of Subzone CN8b of Okada and Bukry (1980), the base of Zone NN10 of Martini (1971), and the base of Zone CNM14 of Backman et al. (2012). The short stratigraphic range of this species at Site 1085 could have affected the precision in the placement of this biohorizon, however, the exit of this taxon documented before the Base absence of *R. pseudoumbilicus*, is consistent with previous literature (Backman and Raffi, 1997; Raffi et al., 2020).

In summary (Fig. 3; Table 1), the presence of *D. hamatus* in the lower part of the study interval indicates that it belongs to Zone CN7, Zone NN9, and Zone CNM13 (Martini, 1971; Okada and Bukry, 1980; Backman et al., 2012). The Base absence of *R. pseudoumbilicus* marks the boundary between Zone CNM14 and CNM15 (Backman et al., 2012), while the appearance of *D. berggrenii* at 467.97 (± 1.85) m indicates the simultaneous start of Zone CN9, Zone NN11, and Zone CNM16 (Martini, 1971; Okada and Bukry, 1980; Backman et al., 2012). The Base of *A. primus* defines the base of Zone CNM17, and the total stratigraphic range of *N. amplificus* marks Zone CNM18 (Backman et al., 2012). The Base common of *D. asymmetricus* marks the top of Zone NN13 and Zone CNPL2 (Okada and Bukry, 1980; Backman et al., 2012), and the disappearance of *R. pseudoumbilicus* defines the base of Zone CN12, Zone NN16 and Zone CNPL4 (Martini, 1971; Okada and Bukry, 1980; Backman et al., 2012).

3.2. Benthic foraminiferal assemblages

Benthic foraminifera are abundant across the studied interval and foraminiferal tests are generally well preserved. A total of 84 taxa (74 calcareous and 10 agglutinated) were recognised at the species or higher taxonomic levels (Suppl. Table S3). Benthic foraminiferal assemblages are strongly dominated by calcareous taxa (e.g. *Bolivina, Epistominella, Globocassidulina*), making up ca. 97.0% of the assemblages throughout most of the studied interval. The Fisher-α diversity index ranges between 11.85 (at 306.42 m) and 27.64 (at 209.00 m). The highest values are reached in the lowermost and uppermost parts of the studied interval and gradually decrease in the middle. The Shannon-Weaver heterogeneity index H(S) ranges between 2.34 and 3.48, with a maximum value in the upper part of the studied interval, at 209.00 m, and its minimum value in the middle part, at 306.42 m.

The relative abundance of phytodetritus exploiting taxa displays a high variability (6.8–50.3% of the assemblages), with the maximum abundance in the middle (385.25 m) and uppermost part of the studied interval. The main component of this group is the species *Epistominella exigua* (Fig. 5.2), followed by *Alabaminella weddellensis* (Fig. 4.4), *Globocassidulina crassa* (Fig. 5.4), and *Globocassidulina subglobosa* (Fig. 5.5). The suboxic-dysoxic group is mainly composed of *Bolivina* spp., *Bulimina* spp. and *Uvigerina* spp., and generally shows an opposite trend to the relative abundance of PET, with the highest abundance (16.6 to 52.1%) between 334.90 and 167.00 m (Fig. 7).

Overall BFARs show low values in the lower and top part of the study interval, and the highest values (>2000) have been recorded between 459.80 and 245.13 m. The coarse fraction (>63 μm) accumulation rates (CFAR) have low values in the lowermost part and highest values between 397.83 and 167.00 m, with a low peak at 240.69 m (Fig. 7).

The hierarchical cluster analysis of species ($n = 21$) shows two main clusters. Cluster A (Fig. 7) contains only *E. exigua*, an epifaunal species that shows large fluctuations in relative abundance (0.0–3.4 to 40.4%), with an increase in relative abundance between 542.45 and 453.49 m, followed by a gradual decrease until 209.00 m, and a secondary increase between 209.00 and 149.00 m.

Cluster B contains 20 species and it is divided into four subclusters. Subcluster B1a is the most diverse one, including six species. The most common species is the epifaunal *Alabaminella weddellensis*, followed by two infaunal species (i.e. *Globocassidulina subglobosa* and *Bulimina truncana*). The relative abundance of this subcluster strongly varies across the studied interval from 5.3% to 51.8%, and it is more abundant in the middle part (between 433.93 and 277.47 m). Subcluster B1b (Fig. 7) includes five species. *Bolivina subaenariensis* (Fig. 4.5) is the most abundant, followed by *Nuttallides umbonifera*, an epifaunal species that increases in the lower part of the study section. The relative abundance of this subcluster ranges from 2.2% to 30.3%. The highest values are documented between 510.23 and 420.60 m, followed by a decrease in the middle part, and a further increase in the upper part, between ca. 299.76 and 191.00 m.

Subcluster B2a (Fig. 7) is the less diverse one, with three infaunal species, *Bolivina spathulata* (Fig. 4.6), *Bulimina elongata* and *Oridorsalis umbonatus* (Fig. 5.9), and the epifaunal *Cibicidoides mundulus*. The relative abundance of Subcluster B2a shows a slight upward decrease, with the highest values between 542.45 and 447.24 m. Subcluster B2b (Fig. 7) includes four infaunal species (*Bulimina striata*, *Cassidulina carapitana*, *Uvigerina peregrina* and *Uvigerina proboscidea*), and the epifaunal *Cibicidoides wuellestorfi*. The most abundant species are *B. striata* (Fig. 4.7) and *U. proboscidea* (Fig. 5.10). The highest relative abundance of this subcluster is reached in the upper part (between 245.13 and 167.00 m). Two minor peaks are present around 453.49 and 528.52 m, due to the increased relative abundance of *C. carapitana* and *U. proboscidea*, respectively.

To further investigate the environmental variables that controlled the benthic foraminiferal distribution pattern, we carried out a DCA analysis in R-mode (species; Suppl. Fig. S1) and Q-mode (samples; Suppl. Fig. S2) on the same dataset as the cluster analysis (species >5% in relative abundance). In the R-mode (species) DCA analysis, species have been grouped into subclusters differentiated in the hierarchical cluster analysis. As a general trend, species are more spread along Axis 2, with species from subcluster B2b at high values, cluster A and subclusters B1b and B2a at intermediate values, and subcluster B1a towards lower values along this axis. We identified only one outlier (*Bolivina spathulata*) that falls outside the 95% confidence ellipse.

4. The Late Miocene-Early Pliocene at Site 1085

4.1. Age model, sedimentation rates and mass accumulation rates

Our new biostratigraphic data are the base for the new age model generated for Site 1085 (Fig. 8; Suppl. Table S6). Our results are substantially different if compared with shipboard data (Wefer et al., 1998), which were used by Westerhold et al. (2005) to build an astronomically calibrated age model from 13.9 to 7.3 Ma, obtained by tuning a high-resolution composite XRF-Fe intensity record of Sites 1085 and 1087. The two models show large differences in the interval between 526.87 and 403.49 m (ca. between 10.5 and 7.0 Ma). In the new data, we identified a gradual increase in the LSR, consistent with the onset of the BB. In contrast, previous results indicated decreased LSRs, which were linked to a decrease in carbonate production, the so-called “Carbonate Crash” event (Westerhold, 2003). The refined biostratigraphy suggests that the orbital age model of Vidal et al. (2002) and Westerhold et al. (2005) should be revised between 11.0 and 7.0 Ma (Fig. 8). As this is a complex and time-consuming endeavour, and not relevant to the findings of this study, we refrain from revising the orbital age model in this study. However, our revised biostratigraphy could be used for the foundation of a future astrochronology. Our results are also a warning sign for taking shipboard stratigraphy for granted, and we recommend checking its reliability whenever possible.

The new biostratigraphic age model provided is constructed based on several tie-points, combining the shipboard and new biostratigraphic data, and it spans from 13.6 (Middle Miocene) to 1.9 Ma (Early Pleistocene). Between two successive tie-points, the sedimentation rate is assumed to have remained constant. The time scale used is the Geological Time Scale 2020 (GTS2020; Raffi et al., 2020) and is based on calcareous nannofossil biochronology provided in GTS2020. The positions of the calcareous nannofossil events from this study have been used

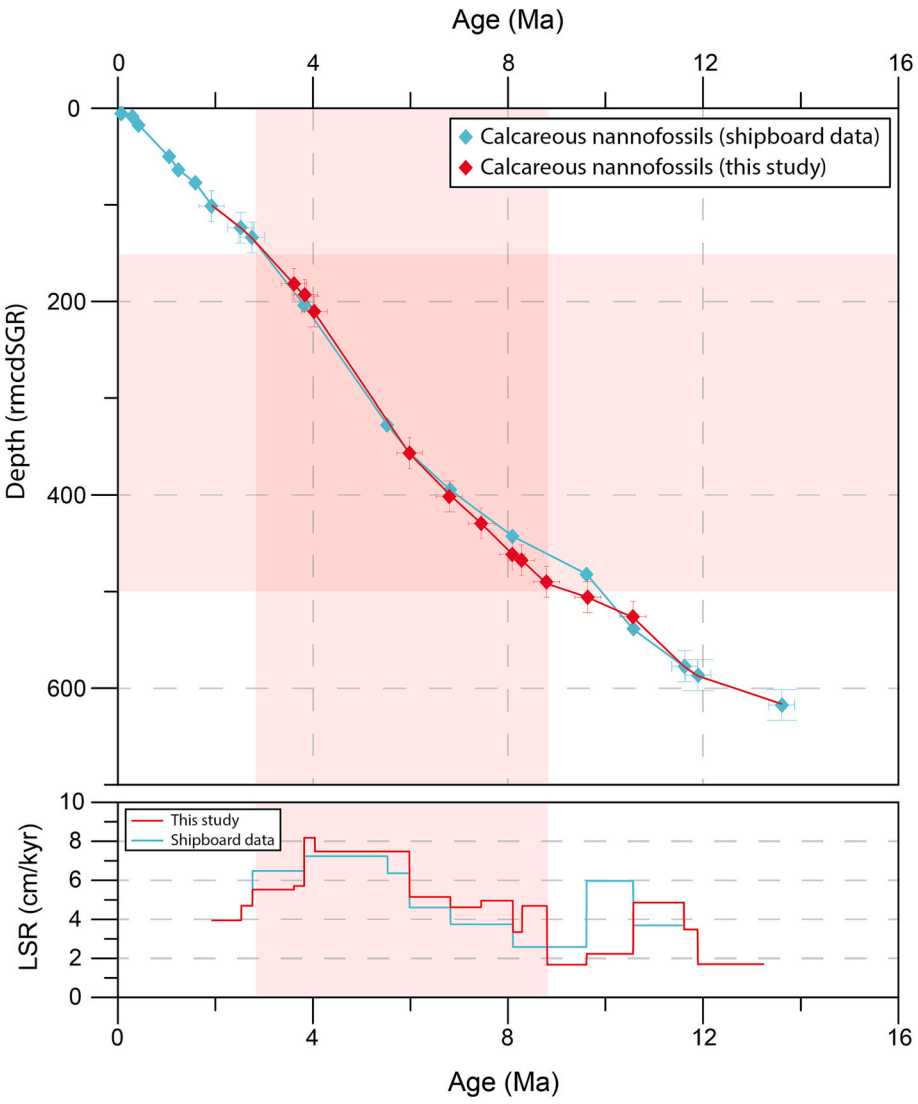

Fig. 8. Age model and linear sedimentation rates at ODP Site 1085. Light blue: shipboard data (Wefer et al., 1998; Westerhold et al., 2005). Red: this study, including error bars. Highlighted in light red: the Biogenic Bloom interval. (For interpretation of the references to colour in this figure legend, the reader is referred to the web version of this article.)

as tie-points to develop the age model between 526.87 and 182.00 m (ca. 10.6–3.6 Ma). Not all biohorizons identified and described in Section 3.1 have been taken into consideration, in particular, the Top *A. primus,* the Top of *D. quinqueramus,* and the Top Absence of *R. pseudoumbilicus* were excluded due to their low degree of reliability.

Based on this age model, LSRs are relatively low between 13.2 and 8.1 Ma (from 616.2 to 461.7 m), with values around 2–3 cm/kyr. An upward increasing trend is observed between 8.1 and 6.0 Ma (from 461.70 to 357.10 m; mean value 4.9 cm/kyr), with the highest values between 6.0 and 4.5 Ma (from 357.10 to 194.10 m; mean value 7.6 cm/kyr). From 4.0 to 1.9 Ma (194.10–100.60 m), LSRs display an upward gradual decrease reaching values around 4–5 cm/kyr (Fig. 8).

The increase in carbonate mass accumulation rates is one of the most commonly used proxies to identify the presence of the BB event in ocean sites (e.g. Farrell et al., 1995; Zhang et al., 2009; Lyle et al., 2019; Drury et al., 2021). To calculate carbonate mass accumulation rates (MAR_{Carb}) at Site 1085, the carbonate content of our samples was derived from Diester-Haass et al. (2004) data using linear interpolation between 542.45 and 149.00 m. The carbonate mass accumulation rates (MAR_{Carb}, expressed as g cm^{-2} kyr^{-1}) were then calculated for each sample, using the LSR (cm/kyr), the calcium carbonate content (wt% $CaCO_3$) and the dry bulk density (DBD, g/cm^3) interpolated from Diester-Haass et al. (2004).

$$MARCarb = \%wtCaCO_3{*}LSR{*}DBD$$

MAR_{Carb} from this study has been plotted with MAR_{Carb} from Diester-Haass et al. (2004), recalibrated using our age model (Suppl. Table S7). The interval older than 8.1 Ma shows MAR_{Carb} values between 1 and 2 g kyr^{-1} cm^{-2}. MAR_{Carb} consistently mirrors the LSR trend. Between 8.1 and 6.0 Ma, we document a first increase with values between 4 and 5 g kyr^{-1} cm^{-2}, while the highest values are reached between 6.0 and 4.5 Ma (from 5 to 8 g kyr^{-1} cm^{-2}). Afterwards, MAR_{Carb} slightly decreases between 4.5 and 3.0 Ma with values ranging from 3.4 to 6.8 g kyr^{-1} cm^{-2}. We interpret the increase in MAR_{Carb} as the expression of the BB occurring between 8.1 and 3.0 Ma at Site 1085.

4.2. Paleoenvironmental interpretation: Benthic foraminiferal response

To further investigate the paleoenvironmental changes across the BB, we focused on the quantitative analysis of benthic foraminiferal assemblages and differentiated six intervals with paleoenvironmental significance between 10.9 and 3.0 Ma (Fig. 9; Table 2): two intervals pre-BB (1a and 1b) and four intervals during the BB (2a, 2b, 2c, and 2d).

Benthic foraminiferal assemblages show brief, transient shifts that

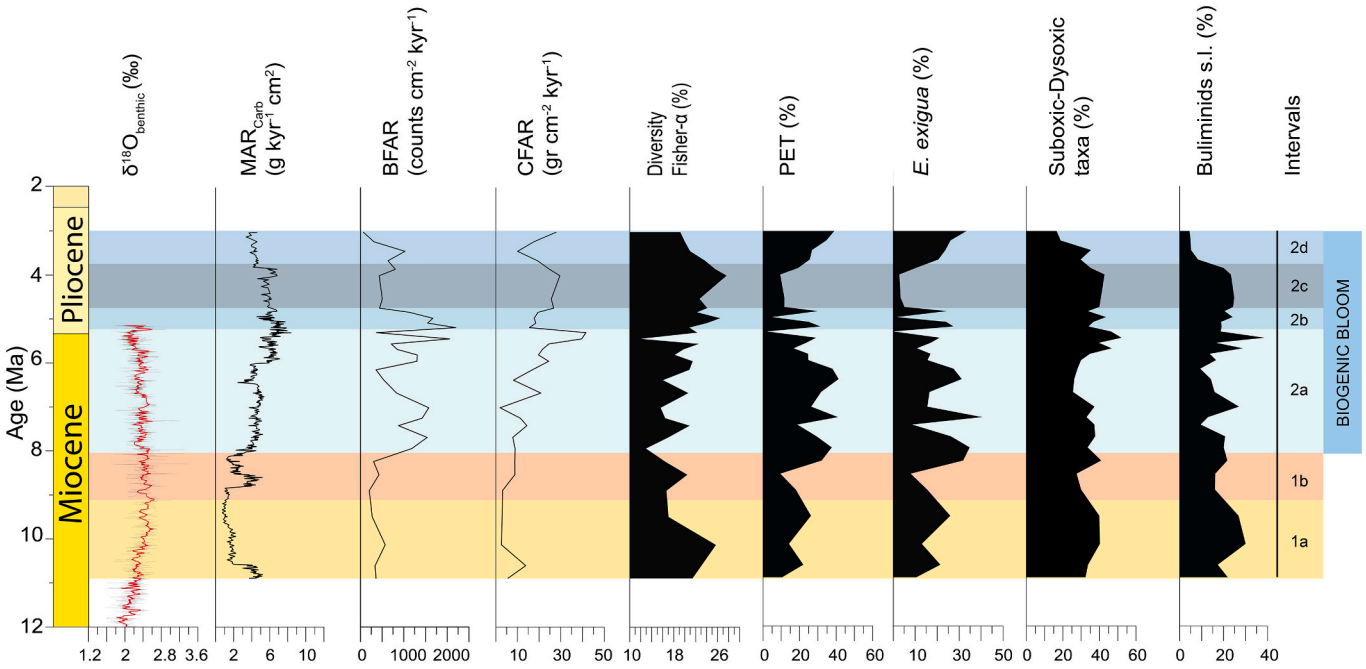

Fig. 9. Benthic stable oxygen isotope records (Westerhold et al., 2005), carbonate mass accumulation rates (MAR_{Carb}), benthic foraminifera accumulation rates (BFAR), coarse fraction accumulation rates (CFAR), diversity (Fisher-α index), relative abundance of phytodetritus exploiting taxa, *Epistominella exigua*, suboxic-dysoxic taxa, and buliminids *s.l.* at ODP Site 1085, plotted against age (Ma).

Table 2
- Summary of the inferred intervals and their paleoenvironmental interpretation across the Late Miocene–Early Pliocene at Site 1085.

	Interval	Depth Range (m)	Age Range (Ma)	Benthic foraminifera assemblage characteristics	Productivity/ oxygenation	Environmental forcing
Pre-Biogenic Bloom (10.9–8.1 Ma)	**1a**	542.45 to 498.46 m	10.9 to 9.2	High diversity, dominance of Subcluster B2a, low BFAR and CFAR, high relative abundance of buliminids s.l., low abundance of oxic species (e.g. *G. subglobosa* and *H. elegans*)	Oxygen depleted conditions at the seafloor with high organic matter fluxes	Increased Orange River's terrestrial runoff which led to a higher influx of terrigenous matter into the ocean. Increased shelf erosion linked to sea level regression due to the expansion of the Antarctic ice sheet
	1b	498.46 to 459.80	9.2 to 8.1	Low diversity, low BFAR. Dominance of subcluster B1b, low abundance of Subcluster B2a, Subcluster B2b, and dysoxic taxa. Peak in relative abundance of *N. umbonifera* and of agglutinated taxa. Large specimens of *G. subglobosa*	Oligotrophic and oxic conditions at the seafloor. Increased carbonate corrosivity	Vertical expansion of the corrosive Upper Circumpolar Deep Water (UCDW) resulting in a reduction of Antarctic Intermediate waters
Biogenic Bloom (8.1–3.0 Ma)	**2a**	459.90 to 287.73	8.1 to 5.2	High LSR, MARCarb and BFAR. Low CFAR. Dominance of Subcluster B1a. High relative abundance of PET and opportunistic taxa (e.g. *A. weddellensis, E. exigua*). Low abundance of suboxic and dysoxic taxa	High oxygen levels and highly seasonal phytodetritus inputs	Expansion of C4 plants, aridification of SW Africa, decrease in precipitation over the African continent, cooling of the Southern Hemisphere. Increased equator-pole temperature gradient and SE trade winds intensification, which led to the intensification of the Benguela upwelling system
	2b	287.73 to 245.13	5.2 to 4.8	Short-term alternations in diversity, BFAR, and in the relative abundance of PET and of suboxic and dysoxic taxa	Short-term alternations between oxic conditions with transient input of phytodetritus and suboxic/dysoxic eutrophic conditions.	Alternations between the expansion of the Antarctic ice sheet with sea level fall and increased continental erosion, and transient warm phases with sea level rise, pulsed upwelling phases and seasonal phytoplankton blooms
	2c	245.13 to 191.00	4.8 to 3.8	Low BFAR and relative abundance of PET. Similar relative abundance in oxic and dysoxic taxa. High abundance of *Bolivina* spp., *Bulimina* spp., *U. peregrina*	No significant changes in oxygen levels. Eutrophic conditions with higher food supply to the seafloor	Warmer climate, poleward shift and a weakening of the Westerlies in both hemispheres. Enhancement of the nutrient-rich and salty Agulhas leakage, which led to ocean stratification and weakening of the upwelling
	2d	191.00 to 149.00	3.8 to 3.0	High abundance of PET, in particular *E. exigua*. Low diversity, low abundance of suboxic and dysoxic taxa	High oxygen concentrations at the seafloor. Seasonal input of phytodetritus due to phytoplankton blooms	Pliocene global cooling trend, increased temperature gradient between the North and South Atlantic, weakened NADW and AMOC. Northward migration of the westerlies, weakening of the Agulhas leakage, and upwelling strengthening

are used to subdivide the study succession into intervals that are characterised by different environmental conditions at the seafloor. *Epistominella exigua* is the most common species throughout the studied interval at Site 1085. This species defines Cluster A and it shows a progressive increase in relative abundance from the base of the study section upward, reaching maximum values during the BB interval. *Epistominella exigua* has been reported to have an opportunistic behaviour, and it increases rapidly in abundance during periods of episodic input of organic matter, linked to seasonal phytoplankton blooms in the upper part of the water column (Gooday, 2003; Jorissen et al., 2007; Corliss et al., 2009). The significant changes in the relative abundance of *E. exigua* (Cluster A) during the BB suggest transient changes in the productivity regime, with brief periods of strong seasonality linked to changes in the type of food reaching the seafloor.

Cluster B is subdivided into four subclusters. Subcluster B1a increases in relative abundance between 7.5 and 5.2 Ma, in the middle of the BB. The dominant taxa of this subcluster are *A. weddellensis* and *G. subglobosa*, two PET associated with high oxygenation and oligotrophic conditions interrupted by strongly seasonal rapid fluxes of organic matter due to phytoplankton blooms (Gooday, 1993; Jorissen et al., 2007). Subcluster B1b shows its peaks in abundance in the lower part of the studied interval (from 9.8 and 7.5 Ma) before the BB. *Nuttallides umbonifera* dominates this subcluster and, together with *H. elegans*, points to oxic and oligotrophic conditions at the seafloor. Moreover, *N. umbonifera* has been interpreted as an indicator of cold, corrosive bottom water (Singh et al., 2012).

Subcluster B2a also shows high relative abundance (up to 29.1%) at the base of the study interval, from 10.4 to 9.2 Ma. The latter increase is directly related to a peak in *Bolivina spathulata*, which has been tentatively linked to eutrophic and low oxygen conditions following the genus paleoecological interpretations (Smart et al., 2007). Lastly, Subcluster B2b decreased in relative abundance during the BB interval and increased between 4.8 and 3.1 Ma. The main components of this subcluster are *B. striata*, *U. peregrina*, and *U. proboscidea*. These species point to high productivity conditions, low seasonality, low oxygenation and high input of food to the seafloor (Loubere, 1998; Gupta and Thomas, 1999; Loubere and Fariduddin, 1999; Ohkushi et al., 1999).

DCA analysis in R-mode (species) confirms differences among subclusters (Suppl. Fig. S1; Gastaldello et al., 2023b), which are mainly distributed along Axis 2. Subcluster B2b dominates at high values along Axis 2, with species common in suboxic-dysoxic environments (*B. striata*, *U. peregrina*, *U. proboscidea*). In contrast, Subcluster B1a dominates at low values along Axis 2 and is composed of small taxa such as *A. weddellensis*, *A. asketocomptella*, and *G. subglobosa*, typical of oxygenated environments and episodic input of nutrients to the seafloor.

5. Discussion

5.1. Pre-Biogenic Bloom (10.9–8.1 Ma)

The oldest part of the studied section has been divided into two pre-BB intervals (1a and 1b) (Fig. 9). Interval 1a spans from 10.9 to 9.2 Ma (from 542.45 to 498.46 m, Fig. 9). The general dominance of Subcluster B2a, together with high diversity values, low BFAR and CFAR, and the high relative abundance of buliminids *s.l.,* suggest oxygen-depleted bottom water conditions with high organic matter fluxes. In particular, the dominance of the small and smooth *B. spathulata* over other *Bolivina* species could be an indicator of extremely low oxygen conditions. A similar sequence of species has been documented at Deep Sea Drilling Program (DSDP) Site 608 (North Atlantic) and in Mediterranean cores (Mullineaux and Lohmann, 1981; Cita and Podenzani, 1980; Ross and Kennett, 1984; Thomas, 1986). The hypothesis of low oxygen conditions is also supported by the almost total absence of oxic species such as *G. subglobosa* and *H. elegans* (Kaiho, 1999; Koho et al., 2008), and by the dark colour of the sediments associated with the increase in pyrite abundance observed during this interval (Wefer et al., 1998; Diester-Haass et al., 2004).

During this interval, increased delivery of terrigenous sediments to the ocean by terrestrial runoff of the Orange River has been documented, and it has been related to cooling and sea level regression due to the expansion of the Antarctic ice sheet and consequent increased shelf erosion (Robert et al., 2005). The increasing arid conditions in the mainland could have increased the erosion area of the Orange River (Diester-Haass et al., 2004). All these factors likely increased the delivery of food to the seafloor, according to the low oxygen and eutrophic conditions inferred from benthic foraminifera.

Interval 1a occurs coevally with the so-called "Carbonate Crash", a paleoceanographic event marked by pervasive carbonate dissolution in sediments between 13.0 and 8.0 Ma (Lübbers et al., 2019). The Carbonate Crash is often identified based on a reduction or cessation in carbonate deposition. At Site 1085, we document low LSR and a steep decline in MAR_{Carb} during the Carbonate Crash window. However, the lower $CaCO_3$ percentage at Site 1085 is likely the result of the dilution by terrigenous components rather than dissolution (Diester-Haass et al., 2004). Furthermore, benthic foraminiferal assemblage data indicate an increased influx of organic matter probably related to increased terrigenous discharge from the Orange River. Finally, the good preservation of the tests and the dominance of calcareous taxa in the assemblages do not support the hypothesis of enhanced $CaCO_3$ dissolution at the seafloor, at least at intermediate depths.

Interval 1b precedes the BB and spans from 9.2 to 8.1 Ma (498.46 to 459.80 m, Fig. 9). Interval 1b is characterised by lower diversity and BFAR compared to Interval 1a, and by species related to oligotrophic and/or high oxygen conditions, such as *Globocassidulina subglobosa*, *Hoeglundina elegans* and *Nuttallides umbonifera* (Lutze and Coulbourn, 1984; Gooday, 1994; Loubere and Fariduddin, 1999; Schönfeld, 2001; Singh et al., 2012). This paleonenvironmental interpretation is supported by the high relative abundance of Subcluster B1b and the low relative abundance of Subcluster B2a, Subcluster B2b, and dysoxic indicators (i.e. *B. subaenariensis*, *B. truncana* and *U. peregrina*) during this interval.

The peak in relative abundance of *Nuttallides umbonifera* and agglutinated taxa (mainly *Sigmoilina schlumbergeri*) at ca. 8.7 Ma (486.41 m) suggests that Site 1085 was influenced by cold corrosive waters (Bremer and Lohmann, 1982). This could be related to a vertical transient expansion of the corrosive Upper Circumpolar Deep Water (UCDW) at the expense of Antarctic Intermediate waters. The UCDW expansion has been used to explain the increase in carbonate dissolution during this time interval, as inferred from the increased the benthic/planktonic foraminifera ratio at Site 1085 (Diester-Haass et al., 2005) and the occurrence of carbonate-depleted sediments at ODP Site 1088 (Diekmann, 2003). An increase in carbonate dissolution is supported by our observation of larger specimens of *G. subglobosa*, particularly at 479.34 m (sample 1085A-49×-2W, 50–52 cm). This increase in size could be related to more favourable living conditions for *G. subglobosa* during this interval (high oxygen and low to intermediate food supply; Gooday, 1994), and/or to increased carbonate corrosivity (Diester-Haass et al., 2004; Diester-Haass et al., 2005). The dissolution would also have had a greater impact on smaller specimens of *G. subglobosa*, preserving the larger specimens in the fossil record.

5.2. The Late Miocene-Early Pliocene Biogenic Bloom (8.1–3.0 Ma)

We identified four different intervals with paleoenvironmental significance during the BB: Intervals 2a, 2b, 2c, and 2d. Interval 2a spans from 8.1 to 5.2 Ma (459.90 to 287.73 m, Fig. 9). It coincides with a first increase in LSR, MAR_{Carb}, and BFAR, low CFAR values, and the dominance of Subcluster B1a. PET and opportunistic taxa dominate the assemblages, with marked peaks at 7.9 Ma (41.4%), 7.2 (47.0%) Ma, and a maximum of 50.0% at 6.0 Ma. The proliferation of this group, predominantly represented by *E. exigua* and *A. weddellensis*, suggests highly seasonal phytodetritus inputs. We observed that during intervals

associated with decreasing diversity and decreasing BFAR (i.e. 7.0 and 6.4 Ma), *E. exigua* shows significant peaks in relative abundance and dominates among PET, while *A. weddellensis* is most abundant when diversity, BFAR, and CFAR increase (i.e. 6.8 and 6.0 Ma). These two species are conventionally used to infer seasonal variations of primary productivity (Sun et al., 2006; Smart, 2008; De Almeida et al., 2015), however, their relative abundance often shows opposite trends in different studies (Thomas et al., 1995; Fariduddin and Loubere, 1997; Sun et al., 2006; Smart, 2008). The high abundance of *A. weddellensis* during higher diversity phases suggests that this species was able to thrive during stable high productivity conditions, while *E. exigua* appears to outcompete other taxa where primary production has a strongly seasonal regime (Sun et al., 2006). The low relative abundance of the dysoxic-suboxic taxa documented during this interval indicates that oxygen concentrations remained uniformly high. Transient decreases in PET (at 5.7 Ma, 7.0 Ma and 7.4 Ma) coincide with peaks in diversity and heterogeneity, and with an increase in infaunal taxa, buliminids and uvigerinids, indicating a temporary shift towards a more constant food flux to the seafloor.

The onset of the BB coincides with the expansion of C4 plants and the increase in δD_{C31} documented at Site 1085 around 8.0–7.0 Ma (Dupont et al., 2013), which have been related to the gradual aridification of western southern Africa. The decrease in precipitation over the African continent during the Late Miocene has been linked to the cooling of the Southern Hemisphere and in particular of the Southern Ocean (Prange and Schulz, 2004; Lunt et al., 2008). These climatic changes led to the increased equator-pole temperature gradient and to intensification of the SE trade winds, which in turn could have resulted in the intensification of the Benguela upwelling system (Berger et al., 2002). Shannon and Nelson (1996) reported that the intensification of the SE trade winds is particularly strong during austral spring and summer in southern Benguela. The high variability in the relative abundance of PET documented during Interval 2a could be a response to seasonal change in the upwelling intensification, with peaks in abundance corresponding to intervals of enhanced upwelling and episodic phytoplankton blooms in surface waters.

Interval 2b spans from 5.2 to 4.8 Ma (287.73 to 245.13 m, Fig. 9) and is characterised by short-term fluctuations in diversity, BFAR, and in the relative abundance of PET and dysoxic-suboxic indicators (e.g. buliminids and uvigerinids). Assemblage census analyses indicate multiple short-term alternations between well-oxygenated conditions with transient pulsed food supply and low-oxygen eutrophic conditions. This interpretation is consistent with the fluctuations recorded in Cluster A and Subclusters B1a and B2b. The sharp increase in the relative abundance of *B. truncana*, the decrease in diversity and in the relative abundance of other buliminids *s.l.* (i.e. *B. elongata*, *B. subaenariensis*, *B. striata*), and the increase in CFAR altogether point to high heterotroph productivity in surface waters and high food supply to the seafloor. The dominance of *B. truncana* over other buliminids species could be related to species-specific preference for particular environmental conditions (i.e. temperature, salinity, type of food).

The short-term oscillation between low oxygen eutrophic conditions and well-oxygenated conditions with seasonal pulsed food supply could be related to sea level changes. Between 6.5 and 5.0 Ma, Kennett (1995) documented a positive shift in $\delta^{18}O$ values associated with the northern migration of the Antarctic ice-rafted detritus front. These changes have been related to an expansion of the Antarctic ice sheet that would have caused a sea level fall. This general trend was interrupted by short transient warm phases associated with sea level rise testified by relatively more negative $\delta^{18}O$ values and the southern migration of the ice-rafted detritus front (Elmstrom and Kennett, 1986; Kennett, 1986; Warnke et al., 1992; Vidal et al., 2002). Sea-level lowstands can enhance the erosion of shelf sediments and increase terrigenous transport by the Orange River. We speculate this mechanism could explain periods of eutrophic conditions marked by the increase in high food supply benthic foraminiferal species. Higher temperatures associated with a potential strengthening of pulsed upwelling phases could be invoked as the mechanism causing the seasonal phytoplankton blooms inferred from the benthic foraminifera assemblage data.

Interval 2c spans from 4.8 to 3.8 Ma (from 245.13 to 191.00 m, Fig. 9) when benthic foraminifera productivity and PET abundance decreased. The decrease in abundance of these opportunistic species likely resulted in the colonization of their ecological niches by other taxa, as documented by the increase in diversity and heterogeneity. The comparable relative abundances of both oxic (i.e. *A. weddellensis*, *C. mundulus*, *G. subglobosa,* subclusters B1a, and B1b; ca. 26.0–30.0%) and dysoxic-suboxic indicators (i.e. *B. subaenariensis*, *B. striata*, *U. peregrina,* subcluster B2b; ca. 35.0–40.0%) suggest that bottom water oxygenation was relatively stable across this interval. The increased abundance of species that better thrived in eutrophic conditions (i.e. *Bolivina* spp., *Bulimina* spp., *U. peregrina*) points to a higher food supply to the seafloor. Interval 2d extends from 3.8 to 3.0 Ma (from 191.00 to 149.00 m, Fig. 8). The return of *E. exigua* as the dominant species in the assemblage, the drop in diversity and the near disappearance of dysoxic-suboxic taxa indicate the return to less eutrophic conditions and high oxygen concentrations. This interval presents conditions similar to the one observed in Interval 2a, in particular, the high abundance of *E. exigua* indicates a strong seasonal component in the primary productivity, and could be associated with recurrent enhancement of the upwelling system.

During the Pliocene, a combination of climatic and tectonic changes influenced the oceanographic conditions (e.g. global warming, decreasing interhemispheric sea surface temperature gradient weakening of the Hadley circulation; Brierley et al., 2009; Karas et al., 2017). Moreover, Abell et al. (2021) inferred a poleward shift and a weakening of the westerlies in both hemispheres as a result of the warmer climate (Brierley et al., 2009). The southward shift in the westerlies could have had a direct impact on Site 1085, enhancing the Agulhas leakage (Durgadoo et al., 2013; Cheng et al., 2018), a source of warm and salty water coming from the Indian Ocean, which in turn resulted in ocean stratification and weakening of the upwelling in the south Benguela regions (Tim et al., 2019). The documented decline of PET, and the inferred reduction of phytoplankton blooms during Interval 2c, could be related to the temporal weakening of the upwelling zone. The enhancement of the nutrient-rich Agulhas leakage (Gordon et al., 1992) could also explain the proliferation of species associated with eutrophic conditions documented during Interval 2c. Between ca. 3.8 and 3.0 Ma, Karas et al. (2017) associated the Pliocene global cooling trend with increased temperature gradient between the North and South Atlantic, and the weakening of the NADW and of the AMOC. These processes led to a northward migration of the westerlies, which in turn, weakened the Agulhas leakage resulting in enhanced upwelling as documented during Interval 2d (Tim et al., 2019).

5.3. The benthic foraminiferal response to the Biogenic Bloom

At Site 1085, increased BFAR and high abundance of PET (mainly *E. exigua* and *A. weddellensis*) suggest that high productivity conditions started at 8.1 Ma. These proxies typically exhibit high variability with short-term oscillations rather than a consistent trend throughout the event, indicating a significant variability and/or seasonality in their driving factors.

The composition of benthic foraminiferal assemblages is controlled by several environmental factors (i.e. bottom water oxygenation, organic matter flux to the seafloor, type and quality of the organic matter, current strength). Local and regional oceanographic, biological and depositional conditions have a significant influence on these factors (Jorissen et al., 2007). At Site 1085, the intensification of the Benguela upwelling system plays a fundamental role in the benthic foraminiferal expression of the BB, leading to seasonal phytoplankton blooms and the dominance of PET in the assemblages. Comparing datasets from different ocean basins could add insight into the benthic foraminiferal

response to the BB, and shed light on local and regional processes and mechanisms behind the event. We compared benthic foraminiferal assemblage data from this study with data from International Ocean Discovery Program (IODP) Site U1506 in the Tasman Sea (southwest Pacific), which spans the Late Miocene-Early Pliocene interval between 7.4 and 4.5 Ma (Gastaldello et al., 2023a). Both Site 1085 and Site U1506 are situated at comparable water depths, with Site 1085 located at a water depth of 1713 m and Site U1506 at 1505 m.

Both sites are dominated by calcareous hyaline taxa. The infaunal/epifaunal ratio is higher at Site U1506, where the dominance of infaunal morphogroups points to eutrophic conditions and/or low oxygen availability at the seafloor. Changes in the relative abundance of suboxic-dysoxic taxa at both sites seem to be related to local changes in oceanography. At Site U1506, Gastaldello et al. (2023a) inferred weak current activity between 6.7 and 4.5 Ma due to the weakening of the East Australian Current (EAC) and shallow-intermediate currents in the Tasman Sea, likely caused by a southward displacement and weakening of the Westerlies and Hadley cell. The weak current activity and high productivity account for the oxygen deficiency. At Site 1085, we did not find any evidence for decreased bottom water oxygenation (i.e. dark organic levels or laminated sediments). The increase in the infaunal/epifaunal ratio and in suboxic-dysoxic taxa is likely related to an increase in nutrient supply.

Phytodetritus exploiting taxa are abundant at both sites, indicating a persisting sinking of phytodetritus along the water column during the BB in both areas (Thomas and Gooday, 1996). Phytodetritus is formed by the accumulation of fresh organic matter (including phytoplankton, cyanobacteria) produced during phytoplankton blooms in the surface waters (Gooday, 2003; Moodley et al., 2002; Gooday et al., 2010). Different species dominate the PET groups at both sites: *E. exigua* and *A. weddellensis* dominate the assemblages at Site 1085, and *G. crassa* and *G. subglobosa* are the most abundant PET at Site U1506. This difference could be caused by the oceanographic conditions at each site. Site 1085 is influenced by the Benguela Upwelling Area, and the increased abundance of the PET group has been associated with phytoplankton blooms with marked seasonality. In contrast, the increase in PET at Site U1506 has been related to the strengthening of the EAC, triggered by the intensification and northward displacement of the westerlies and Hadley cell (Gastaldello et al., 2023a). The intensification of the EAC may account for the arrival of nutrient-rich waters over the site, stronger bottom currents and higher oxygenation at the seafloor, and *G. crassa* and *G. subglobosa* species may have taken advantage of these conditions.

Wind strengthening and oceanographic changes (i.e. increased upwelling, current intensification) during the Late Miocene-Early Pliocene may have played a major role, increasing productivity and triggering phytoplankton blooms in surface waters. More high-resolution quantitative analyses on benthic foraminifera during the Late Miocene to Early Pliocene are fundamental to discern the regional expression of the BB. Crucially, future studies should focus attention on the small size fraction to ensure a comprehensive understanding of benthic foraminiferal assemblages, as PET are commonly missed due to their small size. Finally, high-resolution benthic foraminiferal assemblage studies can also contribute to disentangling global vs. regional species-specific responses.

5.4. The Biogenic Bloom: Was it a global uniform synchronous event?

At a global scale, the available data on the temporal and spatial extent of the BB is still limited or poorly constrained, and, the discussion on the causes and mechanisms behind the BB remains open. The increasing availability of astronomically-tuned and high-resolution records of the BB allows us to speculate about the timing and mechanisms behind the event at a global scale. In the Atlantic Ocean, Drury et al. (2021) documented increased MAR_{Carb} between ca. 7.8 and 3.3 Ma. Data from the Pacific Ocean come from a stack of six sites in the eastern equatorial Pacific (EEP), where the high MAR_{Carb} spans from 8.0 to 4.4 Ma (Lyle et al., 2019), and from Site U1506 in the Tasman Sea, where the event has been documented between 7.4 and 4.5 Ma (Gastaldello et al., 2023a). Previous low-resolution datasets, mostly based on lower-resolution age models, have suggested a scenario in which the onset of the BB is strongly diachronous (e.g. Dickens and Owen, 1999; Hermoyian and Owen, 2001; Grant and Dickens, 2002; Pillot et al., 2023 and references therein). However, comparing the new Site 1085 data with the other high-resolution, well-dated Atlantic and Pacific studies, we observed that the onset of the BB is remarkably synchronous, with the first increase in MAR_{Carb} around ca. 8.0 Ma at Site 1085 (Fig. 10). The apparent delay in the onset (7.4 Ma) at Site U1506 could be related to low sediment recovery in the oldest interval. Our results from Site 1085 confirm that the onset of the BB seems to be relatively well-constrained and synchronous, especially when considered alongside reasonable regional and/or local variations in the manifestation of the event. This clear synchronicity suggests that the possible mechanisms responsible for the BB should be sought among triggers capable of producing rapid large-scale changes.

The timing of the end of the BB is less clear. A recent data compilation of average MAR_{Carb} from ocean drilling records (DSDP, ODP and IODP sites) suggests that the BB extends over 4.0 Ma in the Pacific Ocean, ending abruptly around 2.0 Ma (Pillot et al., 2023). Datasets from the Atlantic and Indian Oceans show a more gradual decrease between 3.5 and 3.0 Ma (Pillot et al., 2023), while Karatsolis et al. (2022) suggest the event ended between ca. 4.6 and 4.4 Ma, documenting a marked decrease in productivity in a global compilation of productivity records, mostly from low-latitude sites. In agreement with the results of Karatsolis et al. (2022), MAR_{Carb} in the Pacific sites seems to indicate that the BB ended at 4.5–4.4 Ma (Lyle et al., 2019; Gastaldello et al., 2023a), while in the Atlantic Ocean, the event seems to extend until 3.3–3.0 Ma (Drury et al., 2021). Our results corroborate the observation that the BB displayed an extended duration in the Atlantic Ocean, ending at ca. 3.0 Ma (Fig. 10). This apparent diachroneity in the ending of the event could be related to regional variability, geographical location and depth of each site, dissolution bias, and differences in the age models but this point remains still highly debatable.

Regarding the mechanisms behind the BB, several explanations for the increased primary productivity have been proposed, ranging from increased nutrient supply due to increased weathering to changes in atmospheric and oceanic circulation patterns affecting global nutrient distribution. (Filippelli, 1997; Dickens and Owen, 1999; Hermoyian and Owen, 2001). The increase in nutrient supply has been related to the uplift of the Himalayas (Wang et al., 2014) and the subsequent intensification of the Indian and Asian monsoon, which would have led to increased weathering and nutrient delivery in the oceans (Filippelli, 1997; Holbourn et al., 2018; Yang et al., 2019). Moreover, increased nutrient input from the continents could also be explained by the intensification of the trade winds and aridification during the Late Miocene (Diester-Haass et al., 2006; Dupont et al., 2013; Herbert et al., 2016). Early studies suggested a major redistribution of nutrients from low-productivity regions in the Atlantic to high-productivity regions in the Indian and Pacific Oceans, associated with changes in the atmosphere and ocean dynamics (Dickens and Owen, 1999). Changes in ocean circulation undoubtedly had a significant impact on the BB, however, this hypothesis is challenged by the global nature of the BB and the increased productivity documented in oligotrophic parts of the Indian Ocean and the South Atlantic Ocean during the Late Miocene-Early Pliocene (Hermoyian and Owen, 2001; Diester-Haass et al., 2005; Drury et al., 2021).

Crucially, the analysis of benthic foraminifera and their paleoenvironmental interpretation indicate that the BB was not a single and continuous, multi-million-year long event (this study, and Gastaldello et al., 2023a). At Site 1085, our findings highlight the regional expression of the BB (Table 2). Changes in the upwelling strength and seasonal phytoplankton blooms during intervals 2a and 2d are reflected in an increase in PET and opportunistic benthic foraminifera. A high

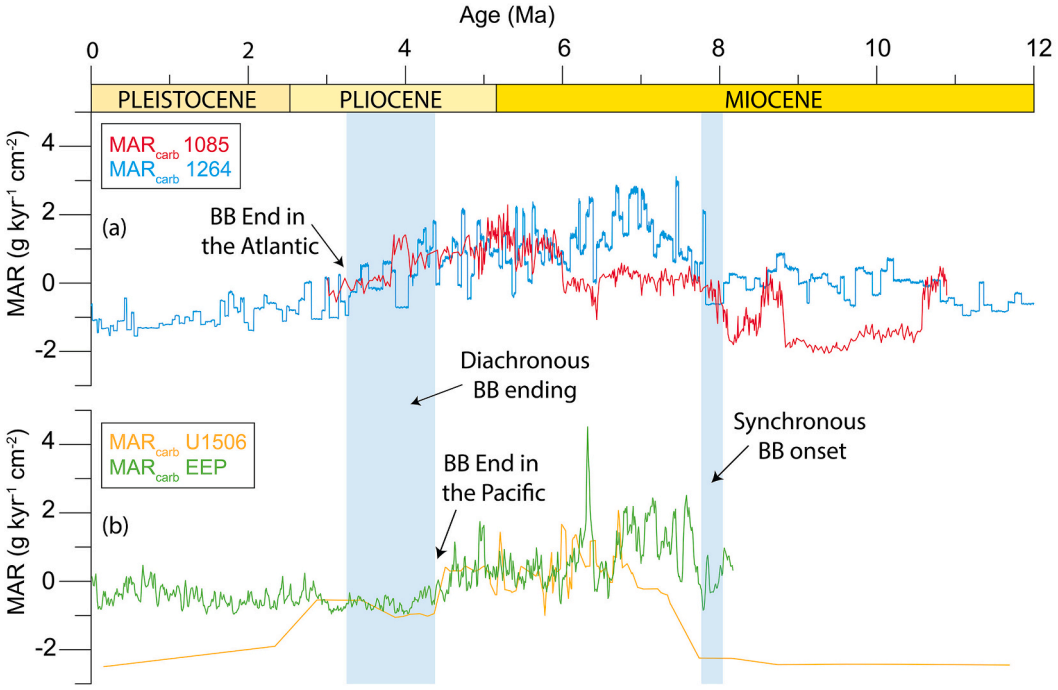

Fig. 10. (a) Normalised MAR_{Carb} of Atlantic sites: ODP Site 1085 (red) and ODP Site 1264 (light blue) (Drury et al., 2021); (b) Normalised MAR_{Carb} of Pacific sites: IODP Site U1506 (orange) (Gastaldello et al., 2023a) and eastern equatorial Pacific stack (EEP, green) (Lyle et al., 2019). (For interpretation of the references to colour in this figure legend, the reader is referred to the web version of this article.)

terrigenous input and the influence of nutrient-rich currents led to eutrophic conditions at the seafloor and to an increase in "high-productivity taxa" such as *Bolivina* and *Bulimina* (Smart et al., 2007), as documented in intervals 2b and 2c. The increasing knowledge on the climatic and tectonic changes that took place during the Late Miocene – Early Pliocene (e.g., Steinthorsdottir et al., 2021) leads us to suggests that multiple driving forces are behind the BB, and that these combined forces influenced its global and regional expression (e.g. global cooling, glacial activity, continental aridity, wind strengthening, opening and/or closing of oceans seaways, changes in equator-pole temperature gradient, monsoon activity).

Approximately 8.0 Ma, the Earth entered a unique regime that allowed for exceptionally high ocean productivity, the Late Miocene to Early Pliocene BB, which persisted for millions of years. Here we show that this extended productivity phase cannot be viewed as a singular productivity event, but instead it was characterised by high variability, and intervals with different productivity regimes were likely related to the dynamics associated with complex biogeochemical cycles. The complex nature of the BB aligns with the impossibility of maintaining consistently high productivity conditions for millions of years, and this interval of enhanced productivity is best understood as the local-to-regional biological response to the significant climatic changes of the Late Miocene-Early Pliocene.

6. Conclusions

This research focused on the Late Miocene-Early Pliocene Biogenic Bloom at SE Atlantic Site 1085. Prior studies conducted on this site were based on problematic age constraints, and benthic foraminifera remained unstudied. New biostratigraphic data allowed us to generate an improve the age model, and the benthic foraminiferal turnover was analysed across the BB, along with additional sedimentary characteristics (LSR, MAR_{Carb}, BFAR).

At Site 1085, the BB spans from 8.1 to 3.0 Ma, based on LSR, MAR_{Carb}, and on benthic foraminiferal assemblage data. Before the BB, we identify two intervals. Interval 1a (10.9–9.2 Ma) represents eutrophic and low oxygen conditions at the seafloor, linked to sea level regression and increased runoff of the Orange River. Interval 1b (9.2–8.1 Ma) is characterised by high oxygen conditions and increased carbonate corrosivity, and it has been related to the expansion of the UCDW. During the BB, we distinguished four intervals that held significance in terms of paleoenvironmental changes. Highly seasonal phytoplankton blooms are inferred from 8.1 to 5.2 Ma (Interval 2a), and from 3.8 to 3.0 Ma (Interval 2d) based on the high BFAR and the high abundance of phytodetritus exploiting taxa, and in particular of *E. exigua*. These conditions suggest increased upwelling, potentially linked to a strengthening of the Benguela Current. Interval 2b (5.2–4.8 Ma) is characterised by short-term oscillations between well-oxygenated conditions with sporadic, brief influxes of food supply, and phases of low oxygen eutrophic conditions. It is hypothesised that these short phases are related to the alternation between sea-level fall caused by the expansion of the Antarctic ice sheet, and sea level rise resulting from short warm phases. Interval 2c (4.8–3.8 Ma) presents a marked decrease in PET and opportunistic species, and an increase in eutrophic taxa, suggesting a steady input of food supply to the seafloor attributed to the influence of the nutrient-rich Agulhas leakage.

Our results indicate that the regional expression of the BB is heavily influenced by the Benguela Upwelling Area at this site. Changes in sea level, the equator to pole temperature, and wind strengthening are some of the factors that could have influenced the upwelling zone. Seasonal upwelling may account for the high abundance of phytodetritus exploiting taxa at this site. We conclude that high-resolution studies are necessary to differentiate the regional versus the global imprint of the BB, and to understand the mechanisms behind this event. This is especially important as we confirm here that the BB cannot be considered as a single productivity event, but rather a complex combination of different productivity regimes in different regions. Although the BB unfolds in different phases with high variability of conditions related to oceanographic and biotic dynamics, it remains a unique event in representing a multimillion-year phase of generally higher productivity conditions in response to the significant climatic changes of the Late Miocene-Early Pliocene.

Supplementary data to this article can be found online at https://doi.org/10.1016/j.palaeo.2024.112040.

CRediT authorship contribution statement

Maria Elena Gastaldello: Conceptualization, Data curation, Investigation, Writing – original draft, Writing – review & editing. **Claudia Agnini:** Conceptualization, Supervision, Writing – review & editing. **Thomas Westerhold:** Investigation, Writing – review & editing. **Anna Joy Drury:** Writing – review & editing. **Laia Alegret:** Conceptualization, Supervision, Writing – review & editing.

Declaration of competing interest

The authors declare that they have no known competing financial interests or personal relationships that could have appeared to influence the work reported in this paper.

Data availability

Data generated in this study are available in the Supporting Information and archived in PANGAEA database (Gastaldello et al., 2023b).

Acknowledgements

This work was funded by University of Padova DOR grant, CARIPARO Ph.D. scholarship, Fondazione Ing. Aldo Gini scholarship, and Grant PID2019-105537RB-I00 funded by MCIN/AEI/10.13039/501100011033 and by "ERDF A way of making Europe." This research used samples and data provided by the International Ocean Discovery Program (IODP). CA received partial funding from the RETURN Extended Partnership, financed by the National Recovery and Resilience Plan – NRRP, Mission 4, Component 2, Investment 1.3 – D.D. 1243 2/8/2022, PE0000005.

References

Abell, J.T., Winckler, G., Anderson, R.F., Herbert, T.D., 2021. Poleward and weakened westerlies during Pliocene warmth. Nature 589 (7840), 70–75.
Agnini, C., Fornaciari, E., Raffi, I., Catanzariti, R., Pälike, H., Backman, J., Rio, D., 2014. Biozonation and biochronology of Paleogene calcareous nannofossils from low and middle latitudes. Newsl. Stratigr. 47 (2), 131–181.
Backman, J., Raffi, I., 1997. Calibration of Miocene nannofossil events to orbitally tuned cyclostratigraphies from Ceara Rise. In: Proceedings of the Ocean ng Program, Scientific Results, Vol. 154, pp. 83–99.
Backman, J., Shackleton, N.J., 1983. Quantitative biochronology of Pliocene and early Pleistocene calcareous nannofossils from the Atlantic, Indian and Pacific oceans. Mar. Micropaleontol. 8 (2), 141–170.
Backman, J., Raffi, I., Rio, D., Fornaciari, E., Pälike, H., 2012. Biozonation and biochronology of Miocene through Pleistocene calcareous nannofossils from low and middle latitudes. Newsl. Stratigr. 45 (3), 221–244.
Berger, W.H., Stax, R., 1994. Neogene carbonate stratigraphy of Ontong Java Plateau (western equatorial Pacific): three unexpected findings. Terra Nova 6 (5), 520–534.
Berger, W.H., Leckie, R.M., Janecek, T.R., Stax, R., Takayama, T., 1993. Neogene carbonate sedimentation on Ontong-Java-Plateau highlights and open questions. In: Proc ODP Sci Res, Vol. 130, pp. 711–744. https://doi.org/10.2973/odp.proc.sr.130.051.1993.
Berger, W.H., Lange, C.B., Wefer, G., 2002. Upwelling History of the Benguela-Namibia System: A Synthesis of Leg 175 Results. Ocean Drill, Program, College Station, Tex.
Berggren, W.A., Kent, D.V., Van Couvering, J.A., 1985. The Neogene: Part 2. Neogene geochronology and chronostratigraphy. In: Snelling, N.J. (Ed.), The Chronology of the Geological Record, Geol. Soc. London Mem, 10, pp. 211–260.
Bernhard, J.M., 1986. Characteristic assemblages and morphologies of benthic foraminifera from anoxic, organic-rich deposits; Jurassic through Holocene. J. Foramin. Res. 16 (3), 207–215. https://doi.org/10.2113/gsjfr.16.3.207.
Boscolo-Galazzo, F., Thomas, E., Giusberti, L., 2015. Benthic foraminiferal response to the Middle Eocene climatic optimum (MECO) in the south-eastern Atlantic (ODP Site 1263). Palaeogeogr. Palaeoclimatol. Palaeoecol. 417, 432–444. https://doi.org/10.1016/j.palaeo.2014.10.004.
Bown, P.R., Young, J.R., 1998. In: Introduction, in Bown, P. R. (Ed.), Calcareous Nannofossil Biostratigraphy, British Micropalaeontology Society Series. Chapman & Hall, London, pp. 1–15.
Bremer, M.L., Lohmann, G.P., 1982. Evidence for primary control of the distribution of certain Atlantic Ocean benthonic foraminifera by degree of carbonate saturation. Deep Sea Res. Part A. Oceanogr. Res. Papers 29 (8), 987–998.
Brierley, C.M., Fedorov, A.V., Liu, Z., Herbert, T.D., Lawrence, K.T., LaRiviere, J.P., 2009. Greatly expanded tropical warm pool and weakened Hadley circulation in the early Pliocene. Science 323 (5922), 1714–1718.
Bytebier, B., Antonelli, A., Bellstedt, D.U., Linder, H.P., 2011. Estimating the age of fire in the Cape flora of South Africa from an orchid phylogeny. Proc. R. Soc. B Biol. Sci. 278 (1703), 188–195.
Cheng, Y., Beal, L.M., Kirtman, B.P., Putrasahan, D., 2018. Interannual Agulhas leakage variability and its regional climate imprints. J. Climate 31 (24), 10105–10121.
Christensen, B.A., Kalbas, J.L., Maslin, M., Murray, R.W., 2002. Paleoclimatic changes in southern Africa during the intensification of Northern Hemisphere glaciation: evidence from ODP Leg 175 Site 1085. Mar. Geol. 180 (1–4), 117–131.
Cita, M.B., Podenzani, M., 1980. Destructive effects of oxygen starvation and ash falls on benthic life: a pilot study1. Quatern. Res. 13 (2), 230–241.
Corliss, B.H., 1985. Microhabitats of benthic foraminifera within deep-sea sediments. Nature 314 (6010), 435–438.
Corliss, B.H., 1991. Morphology and microhabitat preferences of benthic foraminifera from the northwest Atlantic Ocean. Mar. Micropaleontol. 17 (3–4), 195–236. https://doi.org/10.1016/0377-8398(91)90014-W.
Corliss, B.H., Chen, C., 1988. Morphotype patterns of Norwegian Sea deep-sea benthic foraminifera and ecological implications. Geology 16 (8), 716–719. https://doi.org/10.1130/0091-7613.
Corliss, B.H., Brown, C.W., Sun, X., Showers, W.J., 2009. Deep-sea benthic diversity linked to seasonality of pelagic productivity. Deep-Sea Res. I Oceanogr. Res. Pap. 56 (5), 835–841. https://doi.org/10.1016/j.dsr.2008.12.009.
De Almeida, F.K., De Mello, R.M., Costa, K.B., Toledo, F.A., 2015. The response of deep-water benthic foraminiferal assemblages to changes in paleoproductivity during the Pleistocene (last 769.2 kyr), western South Atlantic Ocean. Palaeogeogr. Palaeoclimatol. Palaeoecol. 440, 201–212. https://doi.org/10.1016/j.palaeo.2015.09.005.
Delaney, M.L., Filippelli, G.M., 1994. An apparent contradiction in the role of phosphorus in Cenozoic chemical mass balances for the world ocean. Paleoceanography 9 (4), 513–527. https://doi.org/10.1029/94PA00795.
Dickens, G.R., Barron, J.A., 1997. A rapidly deposited pennate diatom ooze in Upper Miocene-Lower Pliocene sediment beneath the North Pacific polar front. Mar. Micropaleontol. 31 (3–4), 177–182.
Dickens, G.R., Owen, R.M., 1994. Late Miocene-early Pliocene manganese redirection in the central Indian Ocean: expansion of the intermediate water oxygen minimum zone. Paleoceanography 9 (1), 169–181. https://doi.org/10.1029/93PA02699.
Dickens, G.R., Owen, R.M., 1999. The latest Miocene–early Pliocene BB: a revised Indian Ocean perspective. Mar. Geol. 161 (1), 75–91. https://doi.org/10.1016/S0025-3227(99)00057-2.
Diekmann, M., 2003. Species indicator values as an important tool in applied plant ecology–a review. Basic Appl. Ecol. 4 (6), 493–506.
Diester-Haass, L., 1995. Middle Eocene to early Oligocene paleoceanography of the Antarctic Ocean (Maud Rise, ODP Leg 113, Site 689): change from a low to a high productivity ocean. Palaeogeogr. Palaeoclimatol. Palaeoecol. 113 (2–4), 311–334.
Diester-Haass, L., Meyers, P.A., Rothe, P., 1990. Miocene history of the Benguela Current and Antarctic ice volumes: evidence from rhythmic sedimentation and current growth across the Walvis Ridge (Deep Sea Drilling Project Sites 362 and 532). Paleoceanography 5 (5), 685–707.
Diester-Haass, L., Meyers, P.A., Vidal, L., 2002. The late Miocene onset of high productivity in the Benguela current upwelling system as part of a global pattern. Mar. Geol. 180 (1–4), 87–103.
Diester-Haass, L., Meyers, P.A., Bickert, T., 2004. Carbonate crash and biogenic bloom in the late Miocene: Evidence from ODP Sites 1085, 1086, and 1087 in the Cape Basin, southeast Atlantic Ocean. Paleoceanography 19 (1).
Diester-Haass, L., Billups, K., Emeis, K.C., 2005. In search of the late Miocene–early Pliocene "biogenic bloom" in the Atlantic Ocean (Ocean ng Program Sites 982, 925, and 1088). Paleoceanography 20 (4). https://doi.org/10.1029/2005PA001139.
Diester-Haass, L., Billups, K., Emeis, K.C., 2006. Late Miocene carbon isotope records and marine biological productivity: was there a (dusty) link? Paleoceanography 21 (4). https://doi.org/10.1029/2006PA001267.
Drury, A.J., Liebrand, D., Westerhold, T., Beddow, H.M., Hodell, D.A., Rohlfs, N., et al., 2021. Climate, cryosphere and carbon cycle controls on Southeast Atlantic orbital-scale carbonate deposition since the Oligocene (30–0 Ma). Clim. Past 17 (5), 2091–2117.
Dupont, L.M., Linder, H.P., Rommerskirchen, F., Schefuß, E., 2011. Climate-driven rampant speciation of the Cape flora. J. Biogeogr. 38 (6), 1059–1068.
Dupont, L.M., Rommerskirchen, F., Mollenhauer, G., Schefuß, E., 2013. Miocene to Pliocene changes in South African hydrology and vegetation in relation to the expansion of C4 plants. Earth Planet. Sci. Lett. 375, 408–417.
Durgadoo, J.V., Loveday, B.R., Reason, C.J., Penven, P., Biastoch, A., 2013. Agulhas leakage predominantly responds to the Southern Hemisphere westerlies. J. Phys. Oceanogr. 43 (10), 2113–2131.
Elmstrom, K.M., Kennett, J.P., 1986. Late neogene paleoceanographic evolution of site 590-southwest pacific. Initial Rep. Deep Sea Drill. Proj. 90, 1361–1381.
Fariduddin, M., Loubere, P., 1997. The surface ocean productivity response of deeper water benthic foraminifera in the Atlantic Ocean. Mar. Micropaleontol. 32 (3–4), 289–310.
Farinacci, A., Howe, R.W., 1969-2022. The Farinacci & Howe Catalog of Calcareous Nannofossils, 1-26.
Farrell, J.W., Raffi, I., Janecek, T.R., Murray, D.W., Levitan, M., Dadey, K.A., et al., 1995. 35. Late Neogene sedimentation patterns in the eastern equatorial Pacific Ocean. In: Proceedings of the Ocean Drilling Program. Scientific Results, Vol. 138. Ocean Drilling Program, College Station, TX.

Faucher, G., Riebesell, U., Bach, L.T., 2020. Can morphological features of coccolithophores serve as a reliable proxy to reconstruct environmental conditions of the past? Clim. Past 16 (3), 1007–1025.
Filippelli, G.M., 1997. Intensification of the Asian monsoon and a chemical weathering event in the late Miocene–early Pliocene: implications for late Neogene climate change. Geology 25 (1), 27–30.
Fisher, R.A., Corbet, A.S., Williams, C.B., 1943. The relation between the number of species and the number of individuals in a random sample of an animal population. J. Anim. Ecol. 12, 42.
Fontanier, C., Jorissen, F.J., Licari, L., Alexandre, A., Anschutz, P., Carbonel, P., 2002. Live benthic foraminiferal faunas from the Bay of Biscay: faunal density, composition, and microhabitats. Deep-Sea Res. I Oceanogr. Res. Pap. 49 (4), 751–785. https://doi.org/10.1016/S0967-0637(01)00078-4.
Gartner, S., 1992. Miocene nannofossil chronology in the North Atlantic, DSDP Site 608. Mar. Micropaleontol. 18 (4), 307–331.
Gastaldello, M.E., Agnini, C., Westerhold, T., Drury, A.J., Sutherland, R., Drake, M.K., et al., 2023a. The Late Miocene-Early Pliocene Biogenic Bloom: an integrated study in the Tasman Sea. Paleoceanogr. Paleoclimatol. 38 https://doi.org/10.1029/2022PA004565 e2022PA004565.
Gastaldello, M.E., Agnini, C., Westerhold, T., Drury, A.J., Alegret, L., 2023b. Age model, carbonate mass accumulation rates and benthic foraminifera from ODP Site 175-1085. PANGAEA. https://doi.org/10.1594/PANGAEA.962075.
Gooday, A.J., 1988. A response by benthic foraminifera to the deposition of phytodetritus in the deep sea. Nature 332 (6159), 70–73. https://doi.org/10.1038/332070a0.
Gooday, A.J., 1993. Deep-sea benthic foraminiferal species which exploit phytodetritus: characteristic features and controls on distribution. Mar. Micropaleontol. 22 (3), 187–205. https://doi.org/10.1016/0377-8398(93)90043-W.
Gooday, A.J., 1994. The biology of deep-sea foraminifera: a review of some advances and their applications in paleoceanography. Palaios 14–31.
Gooday, A.J., 2003. Benthic foraminifera (Protista) as Tools in Deep-Water Palaeoceanography: Environmental Influences on Faunal Characteristics.
Gooday, A.J., Levin, L.A., Linke, P., Heeger, T., 1992. The role of benthic foraminifera in deep-sea food webs and carbon cycling. In: Rowe, G.T., Pariente, V. (Eds.), Deep-Sea Food Chains and the Global Carbon Cycle. Springer Netherlands, pp. 63–91.
Gooday, A.J., Malzone, M.G., Bett, B.J., Lamont, P.A., 2010. Decadal-scale changes in shallow-infaunal foraminiferal assemblages at the Porcupine Abyssal Plain, NE Atlantic. Deep-Sea Res. II Top. Stud. Oceanogr. 57 (15), 1362–1382.
Gordon, A.L., Weiss, R.F., Smethie, W.M., Warner, M.J., 1992. Thermocline and intermediate water communication between the south Atlantic and Indian oceans. J. Geophys. Res. 97 (C5), 7223–7240. https://doi.org/10.1029/92JC00485.
Grant, K.M., Dickens, G.R., 2002. Coupled productivity and carbon isotope records in the southwest Pacific Ocean during the late Miocene–early Pliocene BB. Palaeogeogr. Palaeoclimatol. Palaeoecol. 187 (1–2), 61–82. https://doi.org/10.1016/S0031-0182(02)00508-4.
Guichard, S., Jorissen, F., Peypouquet, J.P., 1999. Late Quaternary benthic foraminiferal records testifying lateral variability of the Cape Blanc upwelling signal. Comptes Rendus de l'Académie des Sci. –Ser. IIA-Earth Planet. Sci. 329 (4), 295–301.
Gupta, A.K., Thomas, E., 1999. Latest Miocene-Pleistocene productivity and deep-sea ventilation in the northwestern Indian Ocean (Deep Sea Drilling Project Site 219). Paleoceanography 14 (1), 62–73. https://doi.org/10.1029/1998PA900006.
Hammer, Ø., Harper, D., 2005. Paleontological Data Analysis. Blackwell Publishing, Oxford.
Hammer, Ø., Harper, D.A.T., Ryan, P.D., 2001. PAST: Paleontological statistics software package for education and data analysis. Paleontol. Electr. 4 (1), 9. https://palaeo-electronica.org/2001_1/past/issue1_01.htm.
Hayward, B.W., Buzas, M.A., 1979. Taxonomy and paleoecology of Early Miocene benthic foraminifera of Northern New Zealand and the North Tasman Sea. https://doi.org/10.5479/si.00810266.36.1.
Hayward, B.W., Grenfell, H.R., Sabaa, A.T., Neil, H.L., Buzas, M.A., 2010. Recent New Zealand deep-water benthic foraminifera: taxonomy, ecologic distribution, biogeography and use in paleoenvironmental assessment. GNS Science Monograph 26, 363 p. (Lower Hutt New Zealand).
Hayward, B.W., Sabaa, A.T., Grenfell, H.R., Neil, H., Bostock, H., 2013. Ecological distribution of recent deep-water foraminifera around New Zealand. J. Foramin. Res. 43 (4), 415–442. https://doi.org/10.2113/gsjfr.43.4.415.
Herbert, T.D., Lawrence, K.T., Tzanova, A., Peterson, L.C., Caballero-Gill, R., Kelly, C.S., 2016. Late Miocene global cooling and the rise of modern ecosystems. Nat. Geosci. 9 (11), 843–847. https://doi.org/10.1038/ngeo2813.
Herguera, J.C., Berger, W., 1991. Paleoproductivity from benthic foraminifera abundance: Glacial to postglacial change in the west-equatorial Pacific. Geology 19 (12), 1173–1176.
Hermelin, J.O.R., 1989. Pliocene benthic foraminifera from the Ontong-Java plateau (western equatorial Pacific Ocean): faunal response to changing paleoenvironments. Cushman Foundation for Foraminiferal Research Special Publication. 26, 1–143.
Hermoyian, C.S., Owen, R.M., 2001. Late Miocene-early Pliocene BB: evidence from low-productivity regions of the Indian and Atlantic Oceans. Paleoceanography 16 (1), 95–100. https://doi.org/10.1029/2000PA000501.
Holbourn, A., Henderson, A.S., MacLeod, N., 2013. Atlas of Benthic Foraminifera. John Wiley & Sons. https://doi.org/10.1002/9781118452493.
Holbourn, A.E., Kuhnt, W., Clemens, S.C., Kochhann, K.G., Jöhnck, J., Lübbers, J., Andersen, N., 2018. Late Miocene climate cooling and intensification of southeast Asian winter monsoon. Nat. Commun. 9 (1), 1–13. https://doi.org/10.1038/s41467-018-03950-1.
Jones, R.W., Charnock, M.A., 1985. "Morphogroups" of agglutinated foraminifera. Their life positions and feeding habits and potential applicability in (paleo)ecological studies. Rev. Paléobiol. 4 (2), 311–320.
Jorissen, F.J., de Stigter, H.C., Widmark, J.G., 1995. A conceptual model explaining benthic foraminiferal microhabitats. Mar. Micropaleontol. 26 (1–4), 3–15. https://doi.org/10.1016/0377-8398(95)00047-X.
Jorissen, F.J., Fontanier, C., Thomas, E., 2007. Paleoceanographical Proxies Based on Deep-Sea Benthic Foraminiferal Assemblage Characteristics, 1 (07), 10.1016.S1572-5480 (07), 01012-3.
Kaiho, K., 1991. Global changes of Paleogene aerobic/anaerobic benthic foraminifera and deep-sea circulation. Palaeogeogr. Palaeoclimatol. Palaeoecol. 83 (1–3), 65–85.
Kaiho, K., 1999. Effect of organic carbon flux and dissolved oxygen on the benthic foraminiferal oxygen index (BFOI). Mar. Micropaleontol. 37 (1), 67–76.
Kaminski, M.A., Gradstein, F.M., 2005. Atlas of Paleogene Cosmopolitan Deep-Water Agglutinated foraminifera, vol. 10. Grzybowski Foundation.
Karas, C., Nürnberg, D., Bahr, A., Groeneveld, J., Herrle, J.O., Tiedemann, R., Demenocal, P.B., 2017. Pliocene oceanic seaways and global climate. Sci. Rep. 7 (1), 1–8.
Karatsolis, B.T., Lougheed, B.C., De Vleeschouwer, D., Henderiks, J., 2022. Abrupt conclusion of the Late Miocene-Early Pliocene BB at 4.6-4.4 Ma. Nat. Commun. 13 (1), 1–9.
Kennett, J.P., 1986. Miocene to early Pliocene oxygen and carbon isotope stratigraphy in the southwest Pacific, Deep Sea Drilling Project Leg 90. Initial Rep. Deep Sea Drill. Proj. 90, 1383–1411.
Kennett, J.P., 1995. A review of polar climatic evolution during the Neogene, based on the marine sediment record. In: Paleoclimate and Evolution with Emphasis on Human Origins, pp. 49–64.
Koho, K.A., García, R.D., De Stigter, H.C., Epping, E., Koning, E., Kouwenhoven, T.J., Van der Zwaan, G.J., 2008. Sedimentary labile organic carbon and pore water redox control on species distribution of benthic foraminifera: a case study from Lisbon–Setúbal Canyon (southern Portugal). Prog. Oceanogr. 79 (1), 55–82.
Liao, Y., Lyle, M., 2014. Late Miocene to Pleistocene sedimentation and sediment transport on the Cocos Ridge, eastern tropical Pacific Ocean. Mar. Geol. 355, 1–14.
Linder, H.P., 2003. The radiation of the Cape flora, southern Africa. Biol. Rev. 78 (4), 597–638.
Loubere, P., 1998. The impact of seasonality on the benthos as reflected in the assemblages of deep-sea foraminifera. Deep Sea Res. Part Oceanogr. Res. Pap. 45, 409–432.
Loubere, P., Fariduddin, M., 1999. Benthic foraminifera and the flux of organic carbon to the seabed. In: Modern Foraminifera. Springer Netherlands, pp. 181–199.
Lübbers, J., Kuhnt, W., Holbourn, A.E., Bolton, C.T., Gray, E., Usui, Y., Andersen, N., 2019. The middle to late Miocene "Carbonate Crash" in the equatorial Indian Ocean. Paleoceanogr. Paleoclimatol. 34 (5), 813–832.
Lunt, D.J., Valdes, P.J., Haywood, A., Rutt, I.C., 2008. Closure of the Panama Seaway during the Pliocene: implications for climate and Northern Hemisphere glaciation. Climate Dynam. 30, 1–18.
Lutze, G.F., Coulbourn, W.T., 1984. Recent benthic foraminifera from the continental margin of northwest Africa: community structure and distribution. Mar. Micropaleontol. 8 (5), 361–401.
Lyle, M., Drury, A.J., Tian, J., Wilkens, R., Westerhold, T., 2019. Late Miocene to Holocene high-resolution eastern equatorial Pacific carbonate records: stratigraphy linked by dissolution and paleoproductivity. Clim. Past 15 (5), 1715–1739.
Mackensen, A., Schmiedl, G., Harloff, J., Giese, M., 1995. Deep-sea foraminifera in the South Atlantic Ocean: ecology and assemblage generation. Micropaleontology 342–358.
Martini, E., 1971. Standard Tertiary and Quaternary calcareous nannoplankton zonation. Proc. II Planktonic Conf. Roma 739–785.
Mikkelsen, N., 1990. Cenozoic diatom biostratigraphy and paleoceanography of the western equatorial Indian Ocean. In: Proc. ODP, Sci. Results, Vol. 115, pp. 411–432.
Moodley, L., Middelburg, J.J., Boschker, H.T., Duineveld, G.C., Pel, R., Herman, P.M., Heip, C.H., 2002. Bacteria and Foraminifera: key players in a short term deep-sea benthic response to phytodetritus. Mar. Ecol. Prog. Ser. 236, 23–29.
Mullineaux, L.S., Lohmann, G.P., 1981. Late Quaternary stagnations and recirculation of the eastern Mediterranean; changes in the deep water recorded by fossil benthic foraminifera. J. Foramin. Res. 11 (1), 20–39.
Murray, J.W., 1991. Ecology and Paleoecology of benthic foraminifera. Longman.
Murray, J.W., 2000. When does environmental variability become environmental change? The proxy record of benthic foraminifera. In: Environmental Micropaleontology: The Application of Microfossils to Environmental Geology, pp. 7–37.
Murray, J.W., 2006. Ecology and Applications of benthic foraminifera. Cambridge University Press.
Nomura, R., 1995. Paleogene to Neogene deep-sea paleoceanography in the eastern Indian Ocean: benthic foraminifera from ODP Sites 747, 757 and 758. Micropaleontology 251–290.
Ohkushi, K.I., Thomas, E., Kawahata, H., 1999. Abyssal benthic foraminifera from the northwestern Pacific (Shatsky Rise) during the last 298 kyr. Mar. Micropaleontol. 38 (2), 119–147.
Okada, H., Bukry, D., 1980. Supplementary modification and introduction of code numbers to the low-latitude coccolith biostratigraphic zonation (Bukry, 1973; 1975). Mar. Micropaleontol. 5, 321–325. https://doi.org/10.1016/0377-8398(80)90016-X.
Perch-Nielsen, K., 1985. Cenozoic calcareous nannofossils. In: Bolli, H.M., Saunders, J.B., Perch-Nielsen, K. (Eds.), Plankton Stratigraphy. Cambridge University Press, Cambridge, pp. 427–555.
Peterson, R.G., Stramma, L., 1991. Upper-level circulation in the South Atlantic Ocean. Prog. Oceanogr. 26 (1), 1–73.

Peterson, L.C., Murray, D.W., Ehrmann, W.U., Hempel, P., 1992. Cenozoic carbonate accumulation and compensation depth changes in the Indian Ocean. In: Synthesis of Results from Scientific Drilling in the Indian Ocean, 70, pp. 311–333.
Pillot, Q., Suchéras-Marx, B., Sarr, A.C., Bolton, C.T., Donnadieu, Y., 2023. A global reassessment of the spatial and temporal expression of the Late Miocene BB. Paleoceanogr. Paleoclimatol. 38, e2022PA004564 https://doi.org/10.1029/2022PA004564.
Pitcher, G.C., Walker, D.R., Mitchell-Innes, B.A., Moloney, C.L., 1991. Short-term variability during an anchor station study in the southern Benguela upwelling system: phytoplankton dynamics. Prog. Oceanogr. 28 (1–2), 39–64.
Prange, M., Schulz, M., 2004. A coastal upwelling seesaw in the Atlantic Ocean as a result of the closure of the Central American Seaway. Geophys. Res. Lett. 31 (17).
Raffi, I., Flores, J.A., 1995. Pleistocene through Miocene calcareous nannofossils from eastern equatorial Pacific Ocean (Leg 138). In: Proc. ODP, Sci. Results, Vol. 138, pp. 233–286.
Raffi, I., Backman, J., Rio, D., 1998. Evolutionary trends of tropical calcareous nannofossils in the late Neogene. Mar. Micropaleontol. 35 (1–2), 17–41.
Raffi, I., Backman, J., Fornaciari, E., Pälike, H., Rio, D., Lourens, L., Hilgen, F., 2006. A review of calcareous nannofossil astrobiochronology encompassing the past 25 million years. Quat. Sci. Rev. 25 (23–24), 3113–3137.
Raffi, I., Wade, B.S., Pälike, H., Beu, A.G., Cooper, R., Crundwell, M.P., Vernyhorova, Y. V., 2020. The neogene period. In: Geologic Time Scale 2020. Elsevier, pp. 1141–1215.
Rio, D., Fornaciari, E., Raffi, I., 1990. Late Oligocene through early Pleistocene calcareous nannofossils from western equatorial Indian Ocean (Leg 115). In: Proceedings of the Ocean Drilling Program. Scientific Results, Vol. 115. Ocean Drilling Program, College Station, Texas, USA, pp. 175–235.
Robert, C., Diester-Haass, L., Paturel, J., 2005. Clay mineral assemblages, siliciclastic input and paleoproductivity at ODP Site 1085 off Southwest Africa: a Late Miocene–Early Pliocene history of Orange river discharges and Benguela current activity, and their relation to global sea level change. Mar. Geol. 216 (4), 221–238.
Rogers, J., Bremner, J.M., 1991. The Benguela ecosystem, part VII. Marine geological aspects. Oceanogr. Mar. Biol. Ann. Rev. 29, 1–85.
Rommerskirchen, F., Condon, T., Mollenhauer, G., Dupont, L., Schefuss, E., 2011. Miocene to Pliocene development of surface and subsurface temperatures in the Benguela Current system. Paleoceanography 26 (3).
Ross, C.R., Kennett, J.P., 1984. Late Quaternary paleoceanography as recorded by benthonic foraminifera in Strait of Sicily sediment sequences. Mar. Micropaleontol. 8 (4), 315–336.
Schönfeld, J., 2001. Benthic foraminifera and pore-water oxygen profiles: a re-assessment of species boundary conditions at the western Iberian margin. J. Foramin. Res. 31 (2), 86–107.
Shackleton, N.J., Baldauf, J.G., Flores, J.A., Iwai, M., Moore, T.C., Raffi, I., Vincent, E., 1995. Biostratigraphic summary for Leg 138. In: Proceedings of the Ocean Drilling Program. Scientific Results, Vol. 138. Texas A & M University, Ocean Drilling Program, pp. 517–536.
Shannon, L.V., 1985. The Benguela ecosystem I: evolution of the Benguela, physical features and processes. Oceanogr. Mar. Biol. Ann. Rev. 23, 105–182.
Shannon, L.V., Nelson, G., 1996. The Benguela: large scale features and processes and system variability. In: Wefer, G., Berger, W.H., Siedler, G., Webb, D.J. (Eds.), The South Atlantic Present and Past Circulation. Springer-Verlag, Berlin, pp. 163–210.
Singh, R.K., Gupta, A.K., Das, M., 2012. Paleoceanographic significance of deep-sea benthic foraminiferal species diversity at southeastern Indian Ocean Hole 752A during the Neogene. Palaeogeogr. Palaeoclimatol. Palaeoecol. 361, 94–103. https://doi.org/10.1016/j.palaeo.2012.08.008.
Smart, C.W., 2008. Abyssal NE Atlantic benthic foraminifera during the last 15 kyr: Relation to variations in seasonality of productivity. Mar. Micropaleontol. 69 (2), 193–211.
Smart, C.W., Thomas, E., Ramsay, A.T., 2007. Middle–Late Miocene benthic foraminifera in a western equatorial Indian Ocean depth transect: paleoceanographic implications. Palaeogeogr. Palaeoclimatol. Palaeoecol. 247 (3–4), 402–420.
Steinthorsdottir, M., Coxall, H.K., De Boer, Huber, M., Barbolini, N., Bradshaw, C.D., Strömberg, C.A.E., 2021. The Miocene: the future of the past. Paleoceanogr. Paleoclimatol. 36 (4), e2020PA004037 https://doi.org/10.1029/2020PA004037.
Stramma, L., Peterson, R.G., 1989. Geostrophic transport in the Benguela Current region. J. Phys. Oceanogr. 19, 1440–1448.
Suhr, S.B., Pond, D.W., Gooday, A.J., Smith, C.R., 2003. Selective feeding by benthic foraminifera on phytodetritus on the western Antarctic Peninsula shelf: evidence from fatty acid biomarker analysis. Mar. Ecol. Prog. Ser. 262, 153–162.
Summerhayes, C.P., Kroon, D., Rosell-Mele, A., Jordan, R.W., Schrader, H.-J., Hearn, R., Vilanueva, J., Grimalt, J.O., Eglington, G., 1995. Variability in the Benguela Current upwelling system over the past 70,000 years. Progr. Oceanogr. 35, 207–251.
Sun, X., Corliss, B.H., Brown, C.W., Showers, W.J., 2006. The effect of primary productivity and seasonality on the distribution of deep-sea benthic foraminifera in the North Atlantic. Deep-Sea Res. I Oceanogr. Res. Pap. 53 (1), 28–47.
Sutherland, R., Dickens, G.R., Blum, P., Agnini, C., Alegret, L., Asatryan, G., Bhattacharya, J., Bordenave, A., Chang, L., Collot, J., Cramwinckel, M.J., Dallanave, E., Drake, M.K., Etienne, S.J.G., Giorgioni, M., Gurnis, M., Harper, D.T., Huang, H.-H.M., Keller, A.L., Lam, A.R., Li, H., Matsui, H., Morgans, H.E.G., Newsam, C., Park, Y.-H., Pascher, K.M., Pekar, S.F., Penman, D.E., Saito, S., Stratford, W.R., Westerhold, T., Zhou, X., 2019a. Site U1506. In: Sutherland, R., Dickens, G.R., Blum, P., the Expedition 371 Scientists (Eds.), Tasman Frontier Subduction Initiation and Paleogene Climate. Proceedings of the International Ocean Discovery Program, 371: College Station, TX (International Ocean Discovery Program). https://doi.org/10.14379/iodp.proc.371.103.2019.
Sutherland, R., Dickens, G.R., Blum, P., Agnini, C., Alegret, L., Asatryan, G., Bhattacharya, J., Bordenave, A., Chang, L., Collot, J., Cramwinckel, M.J., Dallanave, E., Drake, M.K., Etienne, S.J.G., Giorgioni, M., Gurnis, M., Harper, D.T., Huang, H.-H.M., Keller, A.L., Lam, A.R., Li, H., Matsui, H., Morgans, H.E.G., Newsam, C., Park, Y.-H., Pascher, K.M., Pekar, S.F., Penman, D.E., Saito, S., Stratford, W.R., Westerhold, T., Zhou, X., 2019b. Expedition 371 methods. In: Sutherland, R., Dickens, G.R., Blum, P., the Expedition 371 Scientists (Eds.), Tasman Frontier Subduction Initiation and Paleogene Climate. Proceedings of the International Ocean Discovery Program, 371: College Station, TX (International Ocean Discovery Program). https://doi.org/10.14379/iodp.proc.371.102.2019.
Takayama, T., 1993. Notes on Neogene calcareous nannofossil biostratigraphy of the Ontong Java Plateau and size variations of Reticulofenestra cocoliths. In: Proc. ODP, Sci. Results, vol. 130. Ocean Drilling Program, pp. 179–229.
Thomas, E., 1986. Early to Middle Miocene benthic foraminiferal faunas from DSDP Sites 608 and 610, North Atlantic. Geol. Soc. Lond. Spec. Publ. 21 (1), 205–218.
Thomas, E., Gooday, A.J., 1996a. Cenozoic deep-sea benthic foraminifers: tracers for changes in oceanic productivity? Geology 24 (4), 355–358.
Thomas, E., Booth, L., Maslin, M., Shackleton, N.J., 1995. Northeastern Atlantic benthic foraminifera during the last 45,000 years: changes in productivity seen from the bottom up. Paleoceanography 10 (3), 545–562.
Tim, N., Zorita, E., Emeis, K.C., Schwarzkopf, F.U., Biastoch, A., Hünicke, B., 2019. Analysis of the position and strength of westerlies and trades with implications for Agulhas leakage and South Benguela upwelling. Earth Syst. Dynam. 10 (4), 847–858.
Van Morkhoven, F.P.C.M., Berggren, W.A., Edwards, A.S., Oertli, H.J., 1986. Cenozoic Cosmopolitan Deep-Water benthic Foraminifera. Elf Aquitaine, Pau.
Vidal, L., Bickert, T., Wefer, G., Röhl, U., 2002. Late Miocene stable isotope stratigraphy of SE Atlantic ODP Site 1085: relation to Messinian events. Mar. Geol. 180 (1–4), 71–85.
Wang, C., Dai, J., Zhao, X., Li, Y., Graham, S.A., He, D., Meng, J., 2014. Outward-growth of the Tibetan Plateau during the Cenozoic: A review. Tectonophysics 621, 1–43.
Warnke, D.A., Allen, C.P., Muller, D.W., Hodell, D.A., Brunner, C.A., 1992. Miocene-Pliocene Antarctic glacial evolution: A synthesis of ice-rafted debris, stable isotope, and planktonic foraminiferal indicators, ODP Leg 114. In: The Antarctic Paleoenvironment: A Perspective on Global Change: Part One, 56, pp. 311–326.
Wefer, G., Berger, W.H., Siedler, G., Webb, D.J., Berger, W.H., Wefer, G., 1996. Central themes of South Atlantic circulation. In: The South Atlantic: Present and Past Circulation, pp. 1–11.
Wefer, G., Berger, W.H., Richter, C., Party, S.S., 1998. 13. Site 1085. In: Proc. ODP, Init. Repts., 175: College Station, TX (Ocean Drilling Program), pp. 385–428. https://doi.org/10.2973/odp.proc.ir.175.113.1998.
Westerhold, T., 2003. The Middle Miocene Carbonate Crash: Relationship to Neogene Changes inOcean Circulation and Global Climate (Doctoral dissertation,. Universität Bremen.
Westerhold, T., Bickert, T., Röhl, U., 2005. Middle to late Miocene oxygen isotope stratigraphy of ODP site 1085 (SE Atlantic): new constrains on Miocene climate variability and sea-level fluctuations. Palaeogeogr. Palaeoclimatol. Palaeoecol. 217 (3–4), 205–222.
Yang, R., Yang, Y., Fang, X., Ruan, X., Galy, A., Ye, C., Meng, Q., Han, W., 2019. Late Miocene Intensified Tectonic Uplift and Climatic Aridification on the Northeastern Tibetan Plateau: evidence from Clay Mineralogical and Geochemical Records in the Xining Basin. Geochem. Geophys. Geosyst. 20, 829–851.
Young, J., 1990. Size variation of Neogene Reticulofenestra coccoliths from Indian Ocean DSDP cores. J. Micropalaeontol. 9 (1), 71–85.
Zeeden, C., Hilgen, F., Westerhold, T., Lourens, L., Röhl, U., Bickert, T., 2013. Revised Miocene splice, astronomical tuning and calcareous plankton biochronology of ODP Site 926 between 5 and 14.4 Ma. Palaeogeogr. Palaeoclimatol. Palaeoecol. 369, 430–451.
Zhang, L., Chen, M., Xiang, R., Zhang, L., Lu, J., 2009. Productivity and continental denudation history from the South China Sea since the late Miocene. Mar. Micropaleontol. 72 (1–2), 76–85.